Performance of river biofilm exposed to heavy metals measured with a new micro fluorometer sensor: suitability as a biosensor for online surface water monitoring and best parameter options

Carafa Roberta[1], Nora Exposito Lorenzo[1], Jordi Sierra Llopart[2], Vikas Kumar[1,3], Marta Schuhmacher[1]

[1]Environmental Engineering Laboratory, Departament d'Enginyeria Quimica, Universitat Rovira i Virgili, Av. Països Catalans 26, 43007 Tarragona, Catalonia, Spain.

[2] University of Barcelona Faculty of Pharmacy, Soil Science Unit, Campus Diagonal, Av. de Joan XXIII, 27-31, 08028 Barcelona, Spain

[3]IISPV, Hospital Universitari Sant Joan de Reus, Universitat Rovira I Virgili, Avinguda del Doctor Josep Laporte, 2, 43204 Reus, Spain.

*Corresponding author: roberta.carafa@fundacio.urv.cat

Abstract

River biofilms are a suitable indicator of toxic stress in aquatic ecosystems commonly exposed to various anthropogenic pollutants from industrial, domestic and agricultural sources. Among these pollutants, heavy metals (HMs) are known to interfere with various physiological processes in river biofilm, directly or indirectly related to photosynthetic performance. Nevertheless, only limited toxicological data are available on the mechanisms and toxico-dynamics of heavy metals. Pulse Amplitude Modulated (PAM) fluorometry is a rapid, non-disruptive, well-established technique to monitor toxic responses on photosynthetic performance, fluorescence-kinetics and changes in yield in other non-photochemical processes. In this study, an innovative micro-PAM-sensor is used to test acute and chronic effects of HMs in river biofilm. In addition, a recovery test is performed. The potentially bioavailable fractions of each HM in exposure medium was estimated by modelling their chemical speciation using Visual MINTEQ 3.1, following the suggestions published in recent European regulations. The main aim of this study is to provide a first calibration of the efficiency of the micro PAM sensor that has been integrated into a low-cost in situ monitoring device able to check water quality in a continuous flowing surface water for the assessment of possible contamination events, including effects of heavy metals. Furthermore, this study provides a fast, highly sensitive, cheap and accurate method to test pollutants effects on a complex community and able to give an insight regarding the probable toxicological mechanisms of HMs on photosynthetic performance in the river biofilm.

Highlights

- Chlorophyll-a fluorescence in river biofilms detects short term metals pollution

- Non-Photochemical Quenching is an early warning parameter with exponential dynamics
- Photosynthetic Yield reacts in metal chronic exposure with hormetic behaviour
- Basal fluorescence could be used as an indicator of stress in metal chronic exposure

Keywords

Toxicity, heavy metal, chemical speciation, river biofilm, EC50, surface water monitoring

1. Introduction

Detrimental impacts of micro-pollutants upon freshwater ecosystems and humans exposed to contaminated water and food are well known. Despite the efforts made in the last decades for the implementation of the Water Framework Directive, requiring improvement in waste water treatment and reduction of point and diffuse sources loads, water pollution is still the main cause of water quality deterioration (Nõges et al., 2016). Ecological quality standards for single substances and mixtures have been established but the uncontrolled release of mixtures with unknown composition in waters will continue until the water diagnosis capacity will be incremented. Data from the European Environmental Agency indicate that in 2018, 60% of surface waters in Europe are in bad ecological status. In particular, aquatic environments are highly affected by metal pollution, with copper (Cu), zinc (Zn), arsenic (As), lead (Pb) and nickel (Ni) being some of the most commonly detected contaminants in surface waters (Roig et al., 2015). The occurrence of metal contamination in fluvial ecosystems is commonly due to urban and mining activities occurring in its watershed (Corcoll et al., 2012). The estimation of the total cost of ecological monitoring of surface water in the EU amounted already to 350 million euros (Lawson J., 2005). The implementation of a more intense and complete water monitoring program remains a challenging task. In fact, the main constraint is that the traditional monitoring, based on grab samples, is not economically affordable and not statistically representative in most of the cases. There is a need for improving the diagnosis

capacity of micropollutants and in particular heavy metals loads on EU Rivers and surface waters in general.

River biofilms are sensitive to organic micropollutants (Tiam et al., 2015) such as pesticides (e.g. Guasch et al., 2003; Pesce et al., 2008), and pharmaceuticals (e.g. Proia et al., 2011, 2013; Corcoll et al., 2014) as well as heavy metals (HMs) contamination (e.g., Leguay et al., 2015; Serra et al., 2010; Bonet et al., 2012). Biofilms are considered to be a good bioindicator and a "early warning system": acute pollutants exposure affects functional descriptors such as photosynthesis efficiency or enzyme activity, and chronic exposure lead to changes in community structure (Sabater et al., 2007). Stream biofilms are assemblies of bacteria, algae, diatoms, protozoa and fungi surrounded by extracellular polymeric substances (EPSs) that adhere and develop on the river bed and immersed materials, formed by phototrophic and heterotrophic communities, both of which are characterized by short generation times of hours to days. In lotic freshwater as well as marine ecosystems, periphytic biofilms support basic ecological functions such as primary production and nutrient cycling (Battin et al., 2003). Due to their structural complexity together with the fact that they are the first to interact with dissolved substances, river biofilms are particularly relevant for contamination assessment (Margoum et al., 2015). Several studies showed that toxicants inhibit algal photosynthesis (Schmitt-Jansen & Altenburger, 2008, Barranguet et al., 2003; Pesce et al., 2010; Corcoll et al., 2011) and indicated the sensitivity of the river biofilms to heavy metals (e.g. Corcoll et al., 2012; Guash et al., 2002, Xu et al., 2016; Tuulaikhuu et al., 2015; Boisvert et al., 2007, Miles et al., 1972, etc.). In particular, one of the main effects of metal toxicity is the inhibition of photosynthesis on autotrophic organisms (e.g. Serra et al., 2009; Corcoll et al., 2011).

Photosynthesis efficiency also called photosystem II (PSII) Quantum Yield or photosynthetic yield is the fraction of the calories of radiation absorbed which are stored as calories of chemical potential. Photosynthesis inhibition measurement by pulse-amplitude-modulation

(PAM) fluorometry and the saturation pulse method is based on the fact that light energy captured by photosynthetic pigments can be either: (i) used to drive photosynthesis, (ii) be dissipated as heat, or (iii) emitted as light (fluorescence). An increase in the yield of one process is directly linked to the decrease in the other two. It is, therefore, possible to measure a change in the efficiency of photochemical processes by measuring the yield of chlorophyll (or other pigments) fluorescence (Maxwell and Johnson, 2000 and Schreiber, 2004). The Pulse-Amplitude Modulation (PAM) fluorimeter operates with a specific modulation of the measuring light signal that allows to detect only fluorescence excited by the measuring light. This method has been proved to be very efficient for the detection of effects of metals in microalgae as well as a very wide range of other toxicants (for a review e.g. Kumar et al., 2014). PAM fluorometry applied in assessing short and long term toxic effects on biofilm communities provides several advantages: (1) a combined and rapid evaluation of several functional parameters in parallel, (2) screening of trends over time, (3) observing effects in replication and (4) being non-destructive (Schmitt-Jansen and Altenburger, 2008).

The principal limitation in the field application of this technique is the high variability of biofilm response and the fact that also variables not related to pollution can influence photosynthetic parameters.

The main purpose of the present study was to test and calibrate in the laboratory an innovative micro-PAM-sensor that has been integrated into a low-cost *in situ* monitoring device (Carafa et al., 2020, submitted patent num. 202030285), measuring the effects of heavy metals in river biofilm *in situ* and online. The monitoring device is presented elsewhere (Carafa et al., *in preparation*; Carafa et al., 2020, submitted patent num. 202030285), but some clarifications are needed to better understand the scope of this work. In order to solve the problem of biofilm variability the device incorporates a reference chamber with a purifying filter and a monitoring chamber with an inert filter. Both chambers house a biofilm and a fluorimeter and

measurements from each chamber are compared to identify changes in the aquatic environment. Having a local reference avoids problems on specific biofilm differences and in these conditions it is important to guarantee the use of a biofilm as sensitive as possible. In general, artificial biofilm communities are more resistant and with less biodiversity, for this reason a pristine natural biofilm was selected for toxicity tests in this study. Our scope is to design a cheap and effective protocol identifying best parameters to be checked to detect acute and chronic toxicity due to heavy metals and ranges of sensitivity. Acute and chronic effects after 24-48h and 1 week of exposure were analysed for exposures to 5 HMs: Cu, Zn, As, Pb and Ni. A short time (1 week) recovery tests were performed in order to exclude a fast recovery of the damaged biofilm that could cause more uncertainty in its use as a biosensor for detecting the effects of chemicals on aquatic systems. The HMs toxicity tests performed allowed addressing several issues related to: (i) differences in the toxicity of the selected heavy metals in river biofilms concerning the specific Mode of Action (MoA) and the bioavailability; (ii) dose-response and time response of Chl-a fluorescence parameters in terms of early warning; (iii) mechanistic information of the selected PAM- parameters.

2. Materials and methods

2.1. Experimental setup and study site

The study was carried out in the Brugent, a calcareous stream tributary of the Francolí River, a Mediterranean river in Tarragona (NE Spain). The Brugent is a typical limestone stream with a basin area of 69 km^2, a mean slope of 2.9%, a mean annual flow of 0.44 m^3s^{-1} and a flood-peak discharge with a 500-year recurrence of 520 m^3s^{-1}(Roca et al., 2009). It is fed by waters of karstic origin, presenting alkaline pH, high concentrations of Ca and Mg, low electrical conductivity and low nutrient and pollutant contents (Roig et al., 2013) (Table 1 in Supplementary material). Colonization of the biofilm was realized on standard 75 by 25 mm microscope glass slides fixed to a stainless steel support during January and February 2019 in

the Brugent River (Fig. 1). Physico-chemical characteristics of the Brugent River were analysed before the study to ensure the good quality of the water, in particular, data from Catalan Water Agency (ACA) surveillance and operational monitoring were analysed (Table 1 in Supplementary material). Values of major indexes of the biological quality of the river from ACA monitoring at the time of this study were: Specific Pollution Sensitivity Index (IPS) (Cemagref, 1982) = 13,4 for phytobenthos, Iberian Biomonitoring Working Party (IBMWP) (Hawkes, 1998) = 225 for macroinvertebrates and Index of Biotic integrity (IBICAT) (de Sostoa et al., 2010) 9,57 for fish. In the laboratory biofilm was maintained under the following conditions: in river water, collected from Brugent River and recirculated with an aquarium pump, in natural solar photoperiod and illumination (maximum irradiance 418 μE m-2 s-1, average day length 14L:10D), pH 6.8 ± 0.1, room temperature (night-day fluctuation, min 15.9 ºC, max 29 ºC st. dev. 4 ºC) and humidity between 22 and 47%. Two days before the starting of the test each slide was carefully transferred in the Petri dish with nutrient-enriched modified Bold's Basal Medium BBM non-autoclaved medium. A liquid modified version of BBM pH 6.8 (Hydrochloric Acid -HCL was used to decreased the pH value to acidic) from Nichols and Bold, 1965 was used for biofilm maintenance: the predominantly inorganic nature of this medium facilitates itself as an axenic-culture maintenance medium.

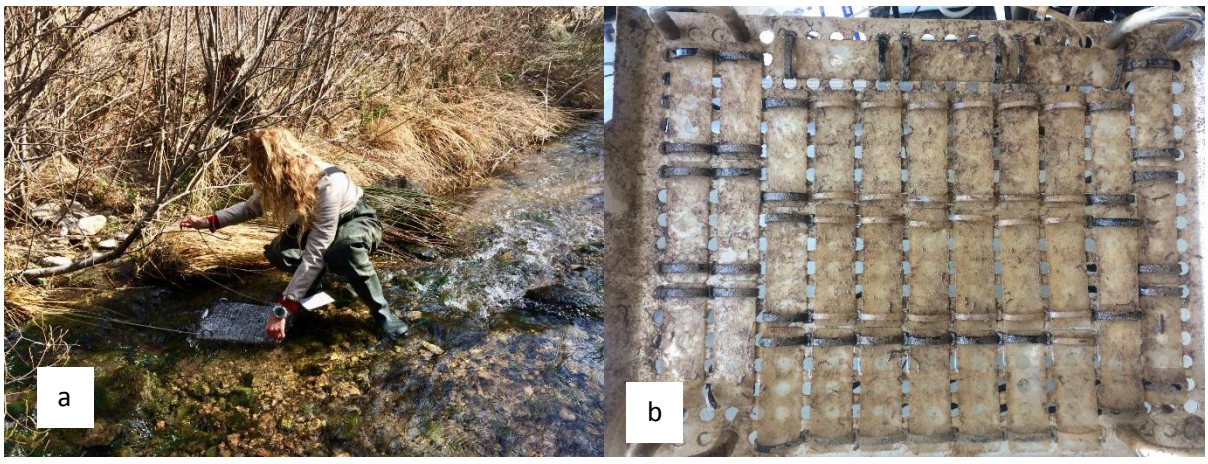

Figure1. Positioning of the glass slides for biofilm colonization in the Brugent River (a) and glass slides after biofilm colonization (b).

2.2. Photosynthesis efficiency inhibition and recovery assays

Effects on photosynthesis efficiency (Pessarakli M, 2016) were tested using micro-PAM instrument (Heinz Walz GmbH, Germany) equipped with LEDs with a wavelength of 470 nm (Supplementary material). The test lasted 2 weeks and was performed in Petri capsules with BBM medium (control) or BBM medium spiked with test substances to a final volume of 25 ml. Media were replaced every two days. All reagents were purchased from Sigma AldrichTM (Saint Louis, MI, USA). Dilutions of single metals were prepared in distilled water (Table 1).

Biofilms were exposed to 7 known concentrations of HMs (Cu, Zn, As, and Ni) ranging from 0.01 mM to 10 mM (spiked volume: 0.25 ml) with exception of Pb where 5 dilutions were prepared due to the lower solubility of this HM (Table 1); 5 blank controls were added to the test battery. In order to measure always the same spot in each slide a numbered grid was added to the bottom of each Petri capsule, as shown in Figure 2. Effects were measured in acute and chronic exposure after 24h, 48h and one-week exposure, and after one-week of recovery. Two sensors were used in parallel to measure two different points in each slide; the sensor measuring heads were placed immersed in the medium perpendicularly at 3.5 mm from the biofilm as shown in Figure 2. The Petri capsule was placed on a stirrer and a stirring bar was added during the test to ensure homogeneous mixing of the HMs in the solution. A box was used to cover the samples for measurements in the dark phase.

After 6 minutes of dark-adaption, minimum fluorescence yield F_0 was measured on non-actinic measuring light (ML) with low intensity (3 µmol quanta $m^{-2}s^{-1}$ PAR, frequency 5 Hz, modulated pulses of 100 µsec). The Gain was adjusted such that in the absence of actinic illumination the fluorescence signal was in the range of minimum 150 – 200 units. The

saturation pulse has an intensity of 7700 µmol quanta m^{-2} s^{-1} PAR and lasts for 600 msec. Maximum fluorescence yield F_m, was measured after dark adaptation. Maximal PS II quantum yield (Max YII) was determined after dark adaptation and it was calculated as Max YII= F_v/F_m where F_v (= F_m-F_0) is the unquenched variable fluorescence. Four saturation pulses were applied each 60 sec maintaining the sample in the dark phase to check homogeneity of the replicates. For acute tests the test substances were added during a short break after pulse 2, maintaining the dark phase. The dark phase was maintained during 3 saturation pulses after the addition of the test substances and early effects on PS II checked in dark. Next, actinic light was applied at two PAR intensities: 25 and (after 5 minutes) 65 µmol quanta m^{-2} s^{-1} and further saturating pulses were given at intervals of 100 sec. to measure the maximal level of fluorescence under illuminated conditions F_m'. The transient fluorescence, F_t, was monitored during the entire duration of the test: 5 minutes dark adaptation plus 15 minutes test (5 minutes in dark plus 5 minutes 25 PAR plus 5 minutes 65 PAR). The effective PS II quantum yield was calculated by the formula: YII = (F_m'-F_0')/F_m', where F_0' is the level of fluorescence immediately before the saturation pulse (3 sec. average). Only spots with a uniform covering of biofilm and basal fluorescence greater than 150-200 units were selected at the beginning of the tests in order to enhance homogeneity. The gain was set to 1 and damping to 2; the other PAM settings were left as fabric default. The Stern-Volmer type non-photochemical fluorescence quenching (NPQ) (Bilger and Björkman, 1990), was calculated as: NPQ = (F_M - $F_{M'}$)/$F_{M'}$.

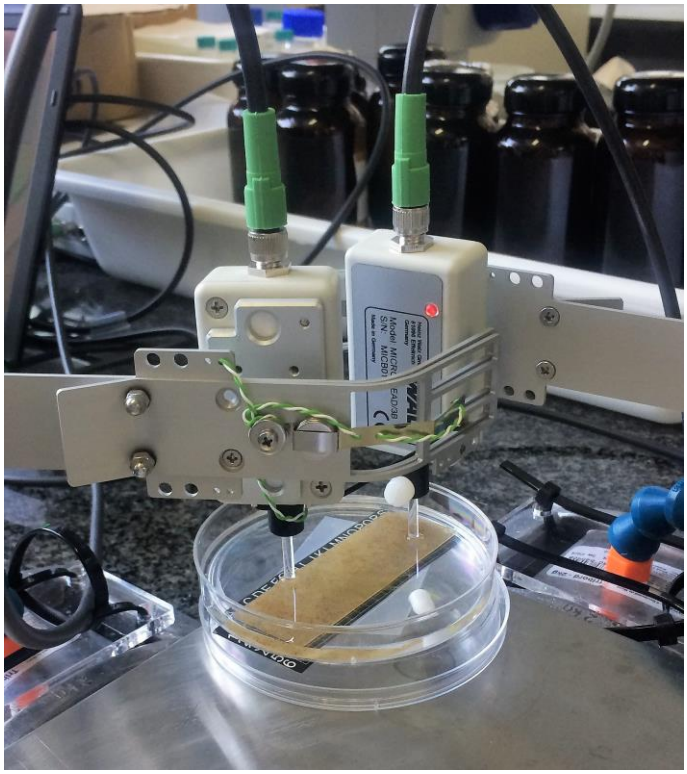

Figure 2. Configuration of laboratory tests: river biofilm on a glass slide (black numbered grill below) and the two micro PAM sensors.

Table 1. Tested single heavy metal dilutions (nominal concentrations in µg L^{-1} and corresponding concentration expressed in mM).

Heavy metal	**As**	**Cu**	**Ni**	**Zn**	**Pb**	**Heavy metal**	**As, Cu, Ni, Zn**	**Pb**
Source	**$HAsNa_2O_4$**	**$CuSO_4$**	**$NiCl_2$**	**$ZnCl_2$**	**$PbCl_2$**			
Tested dilutions (ppb or µg L^{-1})	7.49E+05	6.35E+05	5.87E+05	6.54E+05	4.14E+04	**Tested dilutions (mM)**	10	0.2
	3.75E+05	3.18E+05	2.94E+05	3.27E+05	2.07E+04		5	0.1
	1.50E+05	1.27E+05	1.17E+05	1.31E+05	1.04E+04		2	0.05
	7.49E+04	6.35E+04	5.87E+04	6.54E+04	2.07E+03		1	0.01
	3.75E+04	3.18E+04	2.94E+04	3.27E+04	1.04E+03		0.5	0.005
	1.50E+04	1.27E+04	1.17E+04	1.31E+04			0.2	
	7.49E+02	6.35E+02	5.87E+02	6.54E+02			0.01	

2.3. Biofilm characterization

Biofilms were carefully removed from slides using a razor blade, then suspended in the BBM medium. The proportion of diatoms and chlorophyceae was determined by counting on a Neubauer chamber at the light microscope. The microscopy observations were performed with a magnitude of 100 X, 200 X, 400 X, 500 X for optical confocal microscope identification (Fig. 10, 11, 12) and 5 X to 62 X for stereoscopic microscope (M205 C Stereo Microscope Leica) photos (Fig. 9). Sample preparation and taxonomic identification were performed following European standard NF EN 13946. Diatoms and chlorophyceae were identified to the lowest taxonomic level possible using standard references (John et al., 2002; Handa et al., 2014; Guasch et al., 2002; Bellinger and Sigee, 2010, https://www.algaebase.org) and recent nomenclature updates.

2.4. Data processing

All data were log-transformed prior to data analysis to ensure the normality of data and homogeneity of variances. The results were fitted using the hormetic concentration-response model by Yoshimasu et al. (2015) implemented in Matlab R2017a. Concentration-response graphs were also plotted in Matlab R2017a.

Metal speciation was simulated by Visual MINTEQ 3.1 (Gustafsson, 2014). This model is a chemical equilibrium model for the calculation of metal speciation, solubility equilibria and sorption for natural waters.

3. Results and Discussion

In tables 2, 3 and 4 of the Supplementary material the values of the parameters of all fitted equations as well as the coefficients indicating the goodness of fit are listed.

3.1. Metals speciation

As the medium contains EDTA and other components that can chelate metal ions, only metal species which were bioavailable as well as effective concentration and free ions were considered in drawing concentration-response curves. Figure 3 shows the metal species in the different treatment concentrations and the bioavailable species are indicated with colours: in general, EDTA binds with metals and affects the bioavailability only at lower concentrations. Some more specific comments on single metals follow.

Cu, Zn, and Ni showed the most complex behaviours: a) at a lower concentration, they had in common a high sequestration rate by EDTA, and decreasing bioavailability, b) whereas at higher metal concentration, the EDTA was saturated and the most of metals became bioavailable.

For Cu, all species were considered bioavailable except $CuEDTA^{3-}$ and $CuHPO_4$ aq. Serra et al. (2010) found that Cu toxicity in fluvial periphyton was reduced 1.6 times in a test performed with high Soluble Reactive Phosphorus (SRP) concentration (~50 µM). Since it was not expected that the algae would suffer from Phosphorus (P) limitation during exposure under laboratory conditions (low SRP test ~5 µM), the study supported the hypothesis that P-Cu interaction in the media leads to a reduction in Cu bioavailability. For this reason, we excluded from our calculation of EC50s the fraction of P-Cu complexes.

In the case of Zn, dissolved Zn^{2+}, wasthe reactive species considered bioavailable and, acts as a substitute for Mg, which is the central atom of chlorophyll; this mechanism leads to the breakdown of photosynthesis (Zvezdanović and Marković, 2009).

For Ni, Ni^{2+} was the reactive species considered bioavailable. Ni^{2+} is an essential ion for some enzymatic activities in microalgae (Muyssen et al., 2004) but causes damage to aquatic biota at high concentrations (e.g. Martínez-Ruiz and Martínez-Jerónimo, 2015).

Arsenic was dissolved and bioavailable as anions, $HAsO_4^{2-}$ (46.30%) and $H_2AsO_4^-$ (53.70%), the two species had about the same concentration in the medium.

Lead (Pb) formed complex with EDTA as $PbEDTA^{2-}$ with a very high percentage (>99%) up to 2.000 µg L^{-1}, and at higher concentrations (> 10.000 µg L^{-1}) Pb tends to become more bioavailable basically as Pb2+ free lead.

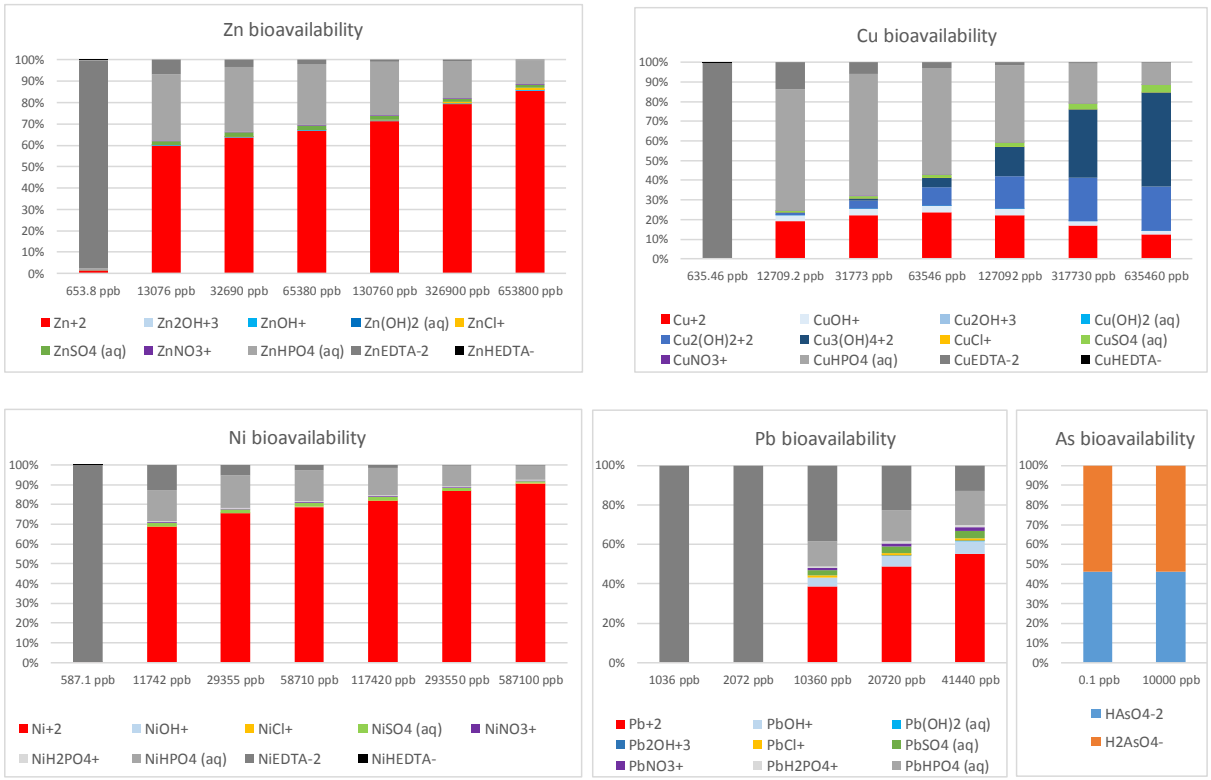

Figure 3. Metal speciation at the different treatment concentrations expressed as % of total metal concentration. Not bioavailable species are indicated with grey shades and bioavailable species with colours. For As only two species present were at equal concentrations for all treatments.

3.2. Non-Photochemical Quenching

Quenching data quantify fluorescence quenching caused by photochemical energy use or non-photochemical energy dissipation. Non-photochemical chlorophyll fluorescence quenching (NPQ) is a process in which excess absorbed light energy is dissipated into heat. This process

takes place in the photosynthetic membranes of photoautotrophs (Demmig-Adams et al., 2014). Figures 4-6 show the results of biofilm exposure to the five investigated metals in dark, 25 PAR and 65 PAR. Table 2 lists the values of the maximum stimulation concentration (hEC) and the logarithm of the half-maximal effective concentration (EC50) of NPQ for Zn, Cu, and Ni.

In acute exposure, immediately after the addition of Zn, Ni, Cu and As an exponential behaviour of the NPQ was observed, while for Pb the data did not show any particular correlation, due to its low bioavailable fraction. These results could be explained considering that stress induced changes in light absorption caused by HMs and could result in loss of excitation energy in the form of heat (Baker et al., 2008), indicated by the increase of the NPQ parameter. Zn, Ni, Cu showed first a stimulation of NPQ at quite high concentrations (log 4 ppb), whereas for As first effects could be detected at log 3 ppb. Light intensity affected the magnitude of the response, when more processes were activated in the cells, the effects of metals appeared more quickly.

The concentration-response curves were very steep for Cu, Zn and Ni in most of the cases probably because of the speciation: at lower concentrations, the bioavailable fraction was reduced (Fig. 3). Chronic tests showed, in most of the cases, a clear hormetic effect (Fig. 4-6).

Zn had a more pronounced hormesis effect after short exposure time (24-48 h); after a week the fitted curves showed a lower stimulation effect, but still, the treatment very close to EC50 showed higher values of NPQ, probably because the cells were actively trying to detoxify (Fig. 4). Autotrophs have various responses to the toxic effects of HMs, such as selective metal uptake, metal binding, and induction of antioxidants (Kycko et al., 2019). After a week in the BBM medium, the biofilms that were exposed to higher Zn concentrations (> log 4 ppb) were able to partially recover (Fig. 4).

Chronic effects of Cu were more pronounced, especially for samples exposed to light, with lower values of EC50 (between log 3 and log 4 ppb; Table 2). In the case of long exposure (one week), the curve became very steep with values of maximum stimulation and EC50 values very close and no recovery after a week of purification was observed.

Ni-exposed samples showed a behaviour very similar to those exposed to Cu, but the EC50 values were higher (> log 4 ppb; Table 2). Also for Ni the samples exposed at higher doses were not able to recover.

As and Pb exposed samples were not negatively affected in any treatment. As seemed to stimulate NPQ after acute, 24 and 48 h exposure (Fig. 5), a tentative exponential curve was drawn also for Pb at 24-48 h and recovery, but the correlation in this last case was very low (Fig. 6).

Due to its fast response after acute exposure (immediately after heavy metal addition), NPQ was identified as an early warning parameter.

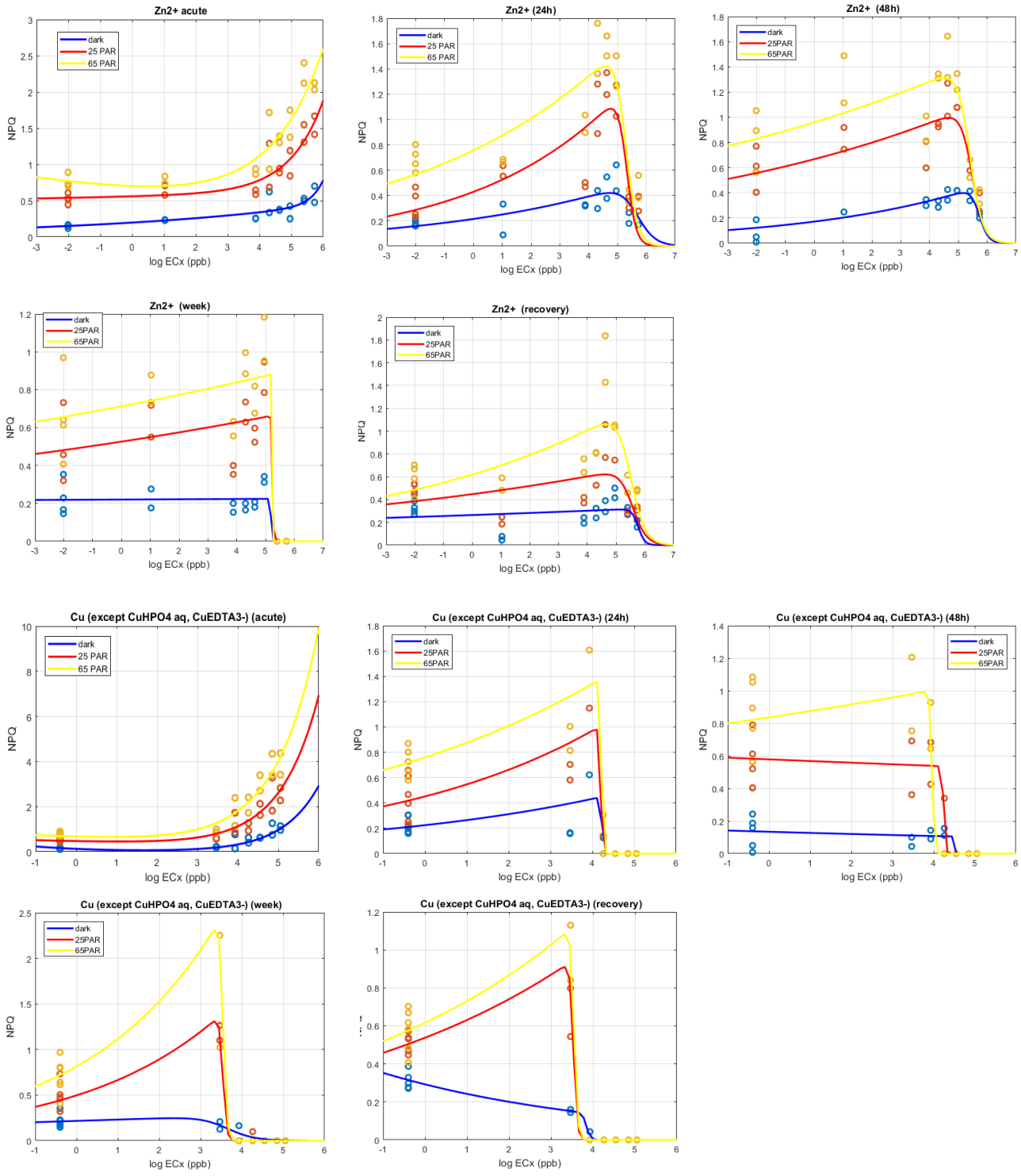

Figure 4. NPQ concentration-response curves (lines) and experimental data (o) for Zinc and Copper exposed samples. Exponential model y = a*exp(b*x) + c*exp(d*x), DFE: 14. Hormetic model y = ((a- b)./(1+(exp((c* x)-d)))./(1+(exp((e*x)- f))). DFE: 12. Fit parameters in Matlab: MaxFunEvals = 6000; MaxIter = 40000; Robust = 'Bisquare'.

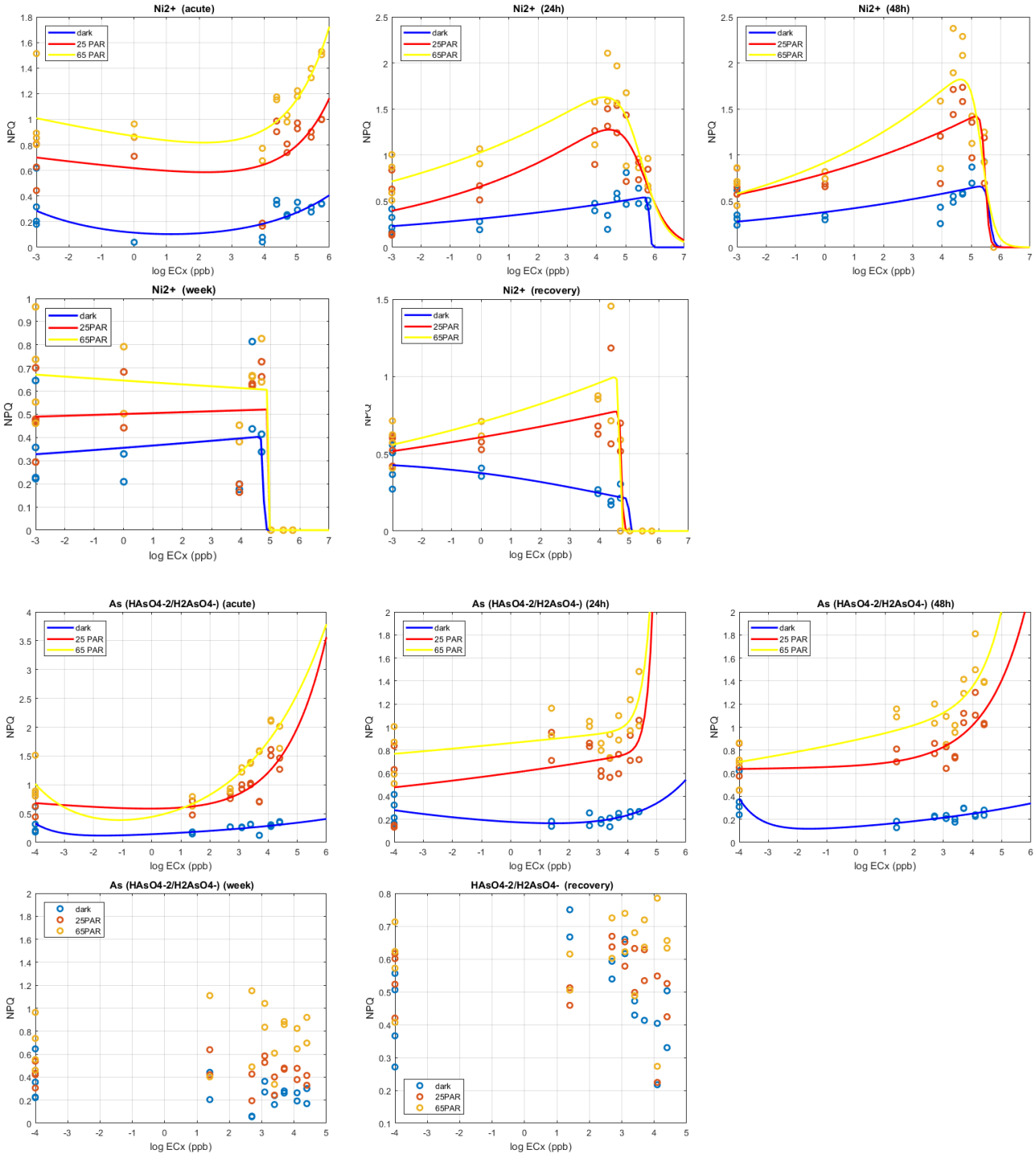

306

307

308 Figure 5. NPQ concentration-response curves (lines) and experimental data (o) for Nickel and

309 Arsenic exposed samples. Exponential model y = a*exp(b*x) + c*exp(d*x), DFE: 14.

310 Hormetic model y = ((a- b)./(1+(exp((c* x)-d)))./(1+(exp((e*x)- f))). DFE: 12. Fit parameters

311 in Matlab: MaxFunEvals = 6000; MaxIter = 40000; Robust = 'Bisquare'.

312

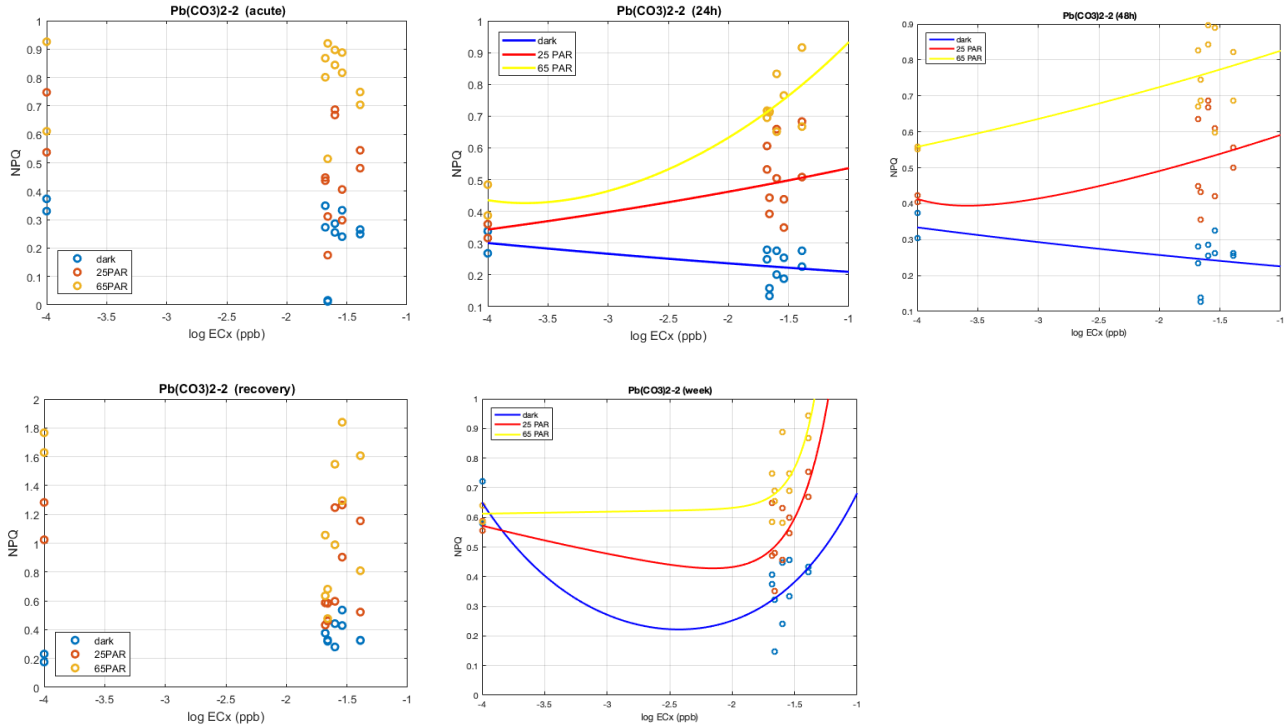

313

314 Figure 6. NPQ concentration-response curves (lines) and experimental data (o) for Lead

315 exposed samples. Exponential model y = a*exp(b*x) + c*exp(d*x), (DFE: 8). MaxFunEvals =

316 6000; MaxIter = 40000; Robust = 'Bisquare'.

317

Table 2. The log maximum stimulated concentration (hEC) and the log half-maximal effective concentration (EC50, ppb) of NPQ for Zn, Cu and Ni on pristine river biofilms. * indicate an exponential fit curve.

NPQ	Zn^{2+} dark		Zn^{2+} (25 PAR)		Zn^{2+} (65 PAR)	
	log hEC	log EC50	log hEC	log EC50	log hEC	log EC50
acute	n.d.*	n.d.*	n.d.*	n.d.*	n.d.*	n.d.*
24h	4.777	6.218	4.770	5.644	4.576	5.593
48h	5.182	5.717	4.677	5.694	4.475	5.576
week	5.081	5.346	5.081	5.295	5.182	5.297
rec	5.182	5.857	4.576	5.785	4.677	5.841
NPQ	Cu (except $CuHPO_4$ aq, $CuEDTA^{3-}$) dark		Cu (except $CuHPO_4$ aq, $CuEDTA^{3-}$)		Cu (except $CuHPO_4$ aq, $CuEDTA^{3-}$)	
	log hEC	log EC50	log hEC	log EC50	log hEC	log EC50
acute	n.d.*	n.d.*	n.d.*	n.d.*	n.d.*	n.d.*
24h	3.889	4.663	4.000	4.071	4.000	4.056
48h	-4.000	3.973	-4.000	3.972	3.778	3.936
week	2.333	3.685	3.333	3.565	3.333	3.667
rec	-4.000	3.424	3.333	3.596	3.333	3.487
NPQ	Ni^{2+} dark		Ni^{2+} (25 PAR)		Ni^{2+} (65 PAR)	
	log hEC	log EC50	log hEC	log EC50	log hEC	log EC50
acute	n.d.*	n.d.*	n.d.*	n.d.*	n.d.*	n.d.*
24h	5.586	5.847	4.475	6.501	4.273	6.108
48h	5.283	5.698	5.182	5.548	4.677	5.699
week	4.576	4.758	4.879	4.959	-3.000	4.605
rec	-3.000	4.166	4.576	4.744	4.475	4.700
NPQ	$HAsO_4^{-2}/H_2AsO_4^-$ dark		$HAsO_4^{-2}/H_2AsO_4^-$ 25PAR		$HAsO_4^{-2}/H_2AsO_4^-$ 65PAR	
	log hEC	log EC50	log hEC	log EC50	log hEC	log EC50
acute	n.d.	n.d.	n.d.*	n.d.*	n.d.*	n.d.*
24h	n.d.*	n.d.*	n.d.*	n.d.*	n.d.*	n.d.*
48h	n.d.	n.d.	n.d.*	n.d.*	n.d.*	n.d.*
week	n.d.	n.d.	n.d.	n.d.	n.d.	n.d.
rec	n.d.	n.d.	n.d.	n.d.	n.d.	n.d.
NPQ	Pb^{2+} dark		Pb^{2+} 25PAR		Pb^{2+} 65PAR	
	log hEC	log EC50	log hEC	log EC50	log hEC	log EC50
acute	n.d.	n.d.	n.d.	n.d.	n.d.	n.d.
24h	n.d.*	n.d.*	n.d.*	n.d.*	n.d.*	n.d.*
48h	n.d.*	n.d.*	n.d.*	n.d.*	n.d.*	n.d.*
week	n.d.*	n.d.*	n.d.*	n.d.*	n.d.*	n.d.*
rec	n.d.	n.d.	n.d.	n.d.	n.d.	n.d.

3.3. Photosynthetic Yield

Results of the measurements of the photosynthetic yield YII are presented in Figure 7. YII was a sensitive parameter, especially in chronic tests (~log 3 ppb) (Fig. 7). The biofilm was highly patchy, but as the YII is derived from a ratio of fluorescence intensities, inhomogeneity of fluorescence excitation intensity or chlorophyll concentration was not be of relevance and remaining inhomogeneity could be interpreted in terms of differences in photosynthetic performance. In Table 3 values of the log maximum stimulation concentration (hEC) and the log half-maximal effective concentration (EC50) of YII for Zn, Cu, Ni, As and Pb are listed. As expected for the YII, light intensity affected positively the magnitude of the response. Again, the hormetic model was used to fit the data but the hormetic effects were much less evident for YII in comparison to NPQ. The complex speciation found for Cu, Zn and Ni can explain the steepness of the curves, in fact, these metals are less bioavailable at a lower concentration, leading to a sudden increase in bioavailability at higher concentrations. The lower photosynthetic performance of the community could depend on the direct toxicity of the metals but could also be attributed to the energetic cost of detoxification (Lavoie et al., 2016).

Zn affected YII in acute exposure when samples were exposed to actinic light, in agreement with his MoA (PSII inhibitor), anyway the effects in acute were very low and the EC50 was > log 7 ppb for samples exposed to 65PAR (Fig. 7; Table 3). The effects of Zn could be seen after 24h, the effects measured after 48 h showed similar behaviour and values of EC50, whereas after a week the curves appeared steeper (Fig. 7; Table 3). Also for YII, samples exposed to Zn were able to recover after one week of depuration (Fig. 7).

Cu exposed samples showed some hormetic effect in acute exposure, this was expected as, even if Cu was toxic at high concentrations, Cu is essential as a component of algal enzymes (e.g. oxidases) and the electron transport chain (e.g. plastocyanin) (Pinto et al., 2003).. The ranges of physiological essential HMs depend on many factors including organism species and

347 the oxidation state of microelement, for example, Mykhaylenko et al. (2017), found that the
348 addition of 0.67-4 mg L^{-1} of Cu nanocarboxylates resulted in the increase in *Chlorella* biomass
349 by ca. 20%; however, their concentrations ranging from 20 to 40 mg L^{-1} strongly inhibited
350 algal growth after the 12th day of cultivation. Similar to Zn, Cu affects YII in acute conditions
351 only when samples were exposed to actinic light, but the effects were evident at lower
352 concentrations in comparison to the effects of the other metals (Fig. 7; Table 3). The steepness
353 of concentration-response curves after chronic exposure of Cu exposed samples were similar
354 for 24-48h and one week exposed samples and also after recovery, but lowest values of EC50
355 were registered in comparison to Zn (Fig. 7; Table 3). In this case, cells were not able to recover
356 and the damage was irreversible.

357 Ni showed also a clear chronic effect on YII with EC50 values at about log 3 ppb at 65 PAR,
358 but no significant acute effect was observed (Fig. 7; Table 3). The lowest EC50 value was
359 registered after one-week exposure, in this case the activation of the photosynthesis seemed
360 slightly mitigate the effects of this metal. At 65 PAR the fit model predicted a hermetic effect
361 at 24 and 48h with hEC at log -2.091 and log -2.394 ppb. Even if the r squared coefficient was
362 high (0.82-0.9, respectively), and Root Mean Square Error (RMSE) was low (0.04-0.04,
363 respectively), no data were available for this part of the curve and other curves does not show
364 this effect. Also for Ni lowest EC50 values are observed after one week of exposure and
365 recuperation was possible only for samples exposed to < log 5 ppb.

366 Small acute and chronic effects were observed for As exposed samples at a very high dose and
367 only during illuminated tests, a complete recovery was observed after a week in clean medium
368 (Fig. 7; Table 3).

369 Finally, for Pb exposed sample not clear response was observed; tentative fitting curves
370 weredrawn, showing a tendency of decrease of YII with higher Pb concentrations, but

bioavailability of this metal was low in all tested concentration, causing assembling of the point and lost in resolution; the Root Mean Square Error (RMSE) was very high (see Supplementary material, Table 3).

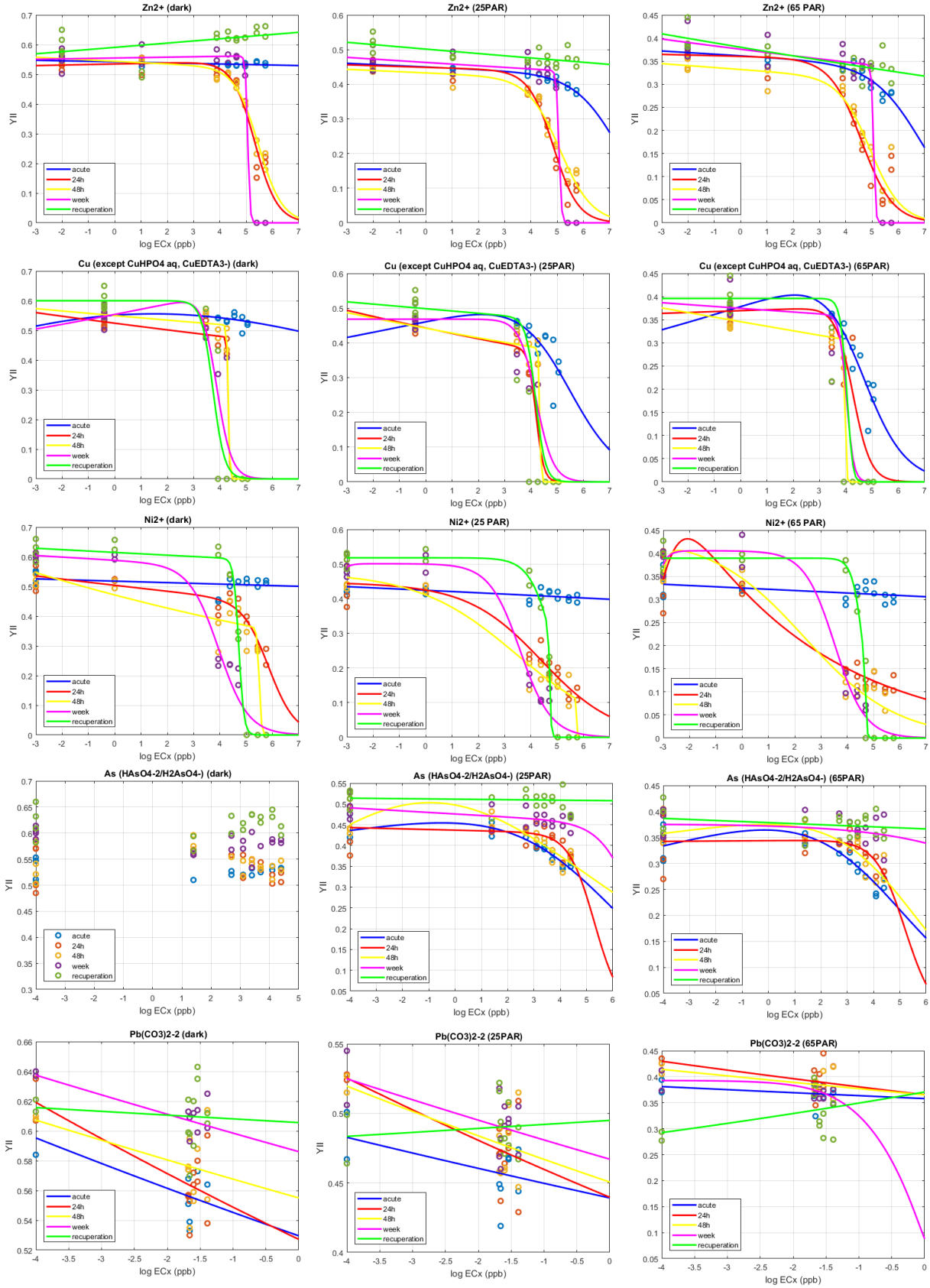

374

375 Figure 7. YII concentration-response curves (lines) and experimental data (o) for Zn, Cu, Ni,

376 As and Pb exposed samples. Hormetic model y = ((a- b)./(1+(exp((c* x)-d)))./(1+(exp((e*x)-

f))). DFE: 12 (DFE 6 for Pb). Fit parameters in Matlab: MaxFunEvals = 6000; MaxIter = 40000; Robust = 'Bisquare'.

Table 3. The log maximum stimulated concentration (hEC) and the log half-maximal effective concentration (EC50, ppb) of YII for Zn, Cu, Ni, As and Pb on pristine river biofilms.

YII	Zn^{2+} dark		Zn^{2+} (25 PAR)		Zn^{2+} (65 PAR)	
	log hEC	log EC50	log hEC	log EC50	log hEC	log EC50
acute	-3.000	n.d.	-3.000	20.266	-3.000	7.055
24h	2.556	5.335	-3.000	4.820	-3.000	4.561
48h	-3.000	5.415	-3.000	5.037	-3.000	4.774
week	4.677	5.029	-3.000	5.048	-3.000	4.285
rec	7.000	n.d.	-3.000	n.d.	-3.000	n.d.
YII	Cu (except $CuHPO_4$ aq, $CuEDTA^{3-}$) dark		Cu (except $CuHPO_4$ aq, $CuEDTA^{3-}$)		Cu (except $CuHPO_4$ aq, $CuEDTA^{3-}$)	
	log hEC	log EC50	log hEC	log EC50	log hEC	log EC50
acute	1.44	24.28	2.15	5.800	2.051	4.958
24h	-3.00	4.58	-3.00	3.871	2.152	3.725
48h	-3.00	3.44	-3.00	4.047	-3	3.787
week	2.56	3.75	-3.00	3.654	-3	3.482
rec	-3.00	3.66	-3.00	3.55	-3	3.48
YII	Ni^{2+} dark		Ni^{2+} (25 PAR)		Ni^{2+} (65 PAR)	
	log hEC	log EC50	log hEC	log EC50	log hEC	log EC50
acute	-3.00	n.d.	-3.00	n.d.	-3	n.d.
24h	-3.00	5.695	-3.00	4.338	-2.091	3.387
48h	-3.00	5.452	-3.00	3.809	-2.394	3.218
week	-3.00	2.610	0.232	3.692	-1.485	3.668
rec	-3.00	4.509	-3.00	4.387	-3	4.348
YII	$HAsO_4^{-2}/H_2AsO_4^-$ dark		$HAsO_4^{-2}/H_2AsO_4^-$ 25PAR		$HAsO_4^{-2}/H_2AsO_4^-$ 65PAR	
	log hEC	log EC50	log hEC	log EC50	log hEC	log EC50
acute	n.d.	n.d.	-0.556	7.063	-0.111	6.123
24h	n.d.	n.d.	-4.000	5.339	1.000	5.376
48h	n.d.	n.d.	-1.000	7.654	-0.120	6.240
week	n.d.	n.d.	-4.000	69.149	-4.000	n.d.
rec	n.d.	n.d.	-4.000	n.d.	-4.000	n.d.
YII	Pb^{2+} dark		Pb^{2+} 25PAR		Pb^{2+} 65PAR	
	log hEC	log EC50	log hEC	log EC50	log hEC	log EC50
acute	-4.00	n.d.	-4.00	n.d.	-4.00	n.d.
24h	-4.00	n.d.	-4.00	n.d.	-4.00	n.d.
48h	-4.00	n.d.	-4.00	n.d.	-4.00	n.d.
week	-4.00	n.d.	-4.00	n.d.	-4.00	-0.323
rec	n.d.	n.d.	n.d.	n.d.	n.d.	n.d.

3.4. Basal fluorescence

According to our results, the basal fluorescence F_0 of dark-adapted cells and F_0' for illuminated samples could also be used as an indicator of stress (Fig. 8 and Table 4; Supplementary materials Table 3). Nevertheless, F_0 measured after dark adaptation and after acute exposure did not show any response in acute tests for any metal, whereas for chronic exposure it seemed to be a good indicator of stress for Zn, Cu, and Ni (Fig. 8).

For Zn chronic exposure F_0 at dark and F_0' for illuminated samples showed similar values, with increasing toxicity when samples were illuminated and with the highest values of EC50 after a week exposure (Fig. 8 and Table 4). Also for this parameter a recovery after a week of purification was observed for Zn.

Cu chronic exposure showed lower values of EC50 in comparison to other metals (Table 4) and no recovery was observed for samples exposed at levels higher than EC50.

For Ni acute effects were very low, no EC50 could be determined in acute, but for chronic exposure, EC50 values were in between those registered for Zn and Cu (Table 4).

For As, only a decreasing tendency of the measured parameters was observed but EC50 could not be calculated (Fig. 8).

Finally, for Pb again no clear effects were observed although the tentative hormetic model predicted some effects for F_0 at a concentration between 0,04 and 0,06 μg/L.

F_0 is directly correlated with Chl a content and thus to biomass in the sample (Eggert et al., 2006), thus theoretically can be used as an endpoint parameter after long-term exposure to detect changes in biofilm biomass. However, we also measured a decrease of F_0 after 24h, which was a short time for detecting changes in biomass. A mechanistic justification of the basal fluorescence results is not easy to formulate, as fluorescence is linked to many

405 physiological processes affected by HMs: stress-induced decreases in stomatal conductance,
406 carbon metabolism, and transport processes can all affect PSII efficiency inducing changes in
407 absorbed light energy use and consequently in fluorescence (Schreiber et al., 2002; Schreiber,
408 2004). In addition, change in the reactive oxygen species (ROS) concentration, causes a change
409 in signal transduction which affects the gene expression, change the properties of the
410 membranes, and also damaging the photosystem II (PSII) (Aro et al., 2005; Miles et al., 1972).
411 Also, these toxic effects induced by HMs may directly or indirectly affect basal fluorescence.

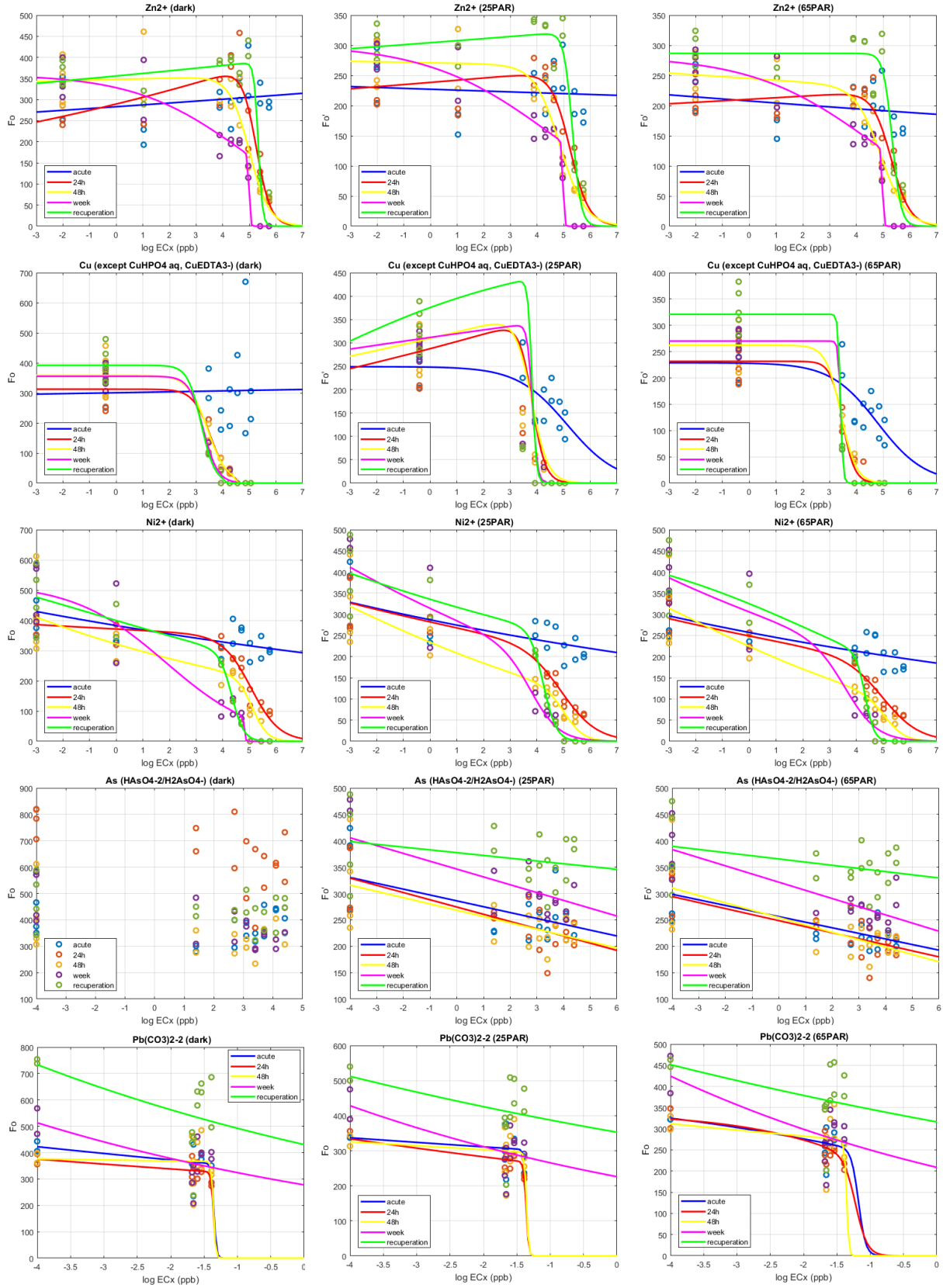

412

413 Figure 8. F_0 concentration-response curves (lines) and experimental data (o) for Zn, Cu, Ni, As

414 and Pb exposed samples. Hormetic model y = ((a- b)./(1+(exp((c* x)-d)))./(1+(exp((e*x)- f))).

415 DFE: 12 (DFE: 6 for Pb). Fit parameters in Matlab: MaxFunEvals = 6000; MaxIter = 40000;

416 Robust = 'Bisquare'.

417 Table 4. The Log maximum stimulated concentration (hEC) and the log half-maximal effective

418 concentration (EC50, ppb) of F_0 for Zn, Cu, Ni, As and Pb on pristine river biofilms.

F_0	**Zn^{2+} dark**		**Zn^{2+} (25 PAR)**		**Zn^{2+} (65 PAR)**	
	log hEC	log EC50	log hEC	log EC50	log hEC	log EC50
acute	n.d.	n.d.	-3.000	n.d.	-3.000	n.d.
24h	4.071	5.413	3.364	5.290	3.364	5.344
48h	2.657	5.006	-3.000	4.836	-3.000	4.512
week	-3.000	4.001	-3.000	4.011	-3.000	3.999
rec	4.778	5.344	4.273	5.345	-3.000	5.337
F_0	**Cu (except $CuHPO_4$ aq, $CuEDTA^{3-}$) dark**		**Cu (except $CuHPO_4$ aq, $CuEDTA^{3-}$)**		**Cu (except $CuHPO_4$ aq, $CuEDTA^{3-}$)**	
	log hEC	log EC50	log hEC	log EC50	log hEC	log EC50
acute	n.d.	n.d.	-3.00	5.29	-3	4.74
24h	-3.000	3.516	2.76	3.449	-3.000	3.451
48h	-3.000	3.447	2.45	3.459	-3	3.444
week	-3.000	3.368	3.26	2.917	-3	2.983
rec	-3.000	3.305	3.36	2.842	-3	2.974
F_0	**Ni^{2+} dark**		**Ni^{2+} (25 PAR)**		**Ni^{2+} (65 PAR)**	
	log hEC	log EC50	log hEC	log EC50	log hEC	log EC50
acute	-3.00	n.d.	-3.00	n.d.	-3	n.d.
24h	-3.00	4.839	-3.00	4.439	-3	4.455
48h	-3.00	4.312	-3.00	3.933	-3	3.882
week	-3.00	4.289	-3.00	3.523	-3	3.541
rec	-3.00	2.984	-3.00	3.998	-3	3.956
F_0	**$HAsO_4^{-2}/H_2AsO_4^-$ dark**		**$HAsO_4^{-2}/H_2AsO_4^-$ 25PAR**		**$HAsO_4^{-2}/H_2AsO_4^-$ 65PAR**	
	log hEC	log EC50	log hEC	log EC50	log hEC	log EC50
acute	n.d.	n.d.	n.d.	n.d.	n.d.	n.d.
24h	n.d.	n.d.	n.d.	n.d.	n.d.	n.d.
48h	n.d.	n.d.	n.d.	n.d.	n.d.	n.d.
week	n.d.	n.d.	n.d.	n.d.	n.d.	n.d.
rec	n.d.	n.d.	n.d.	n.d.	n.d.	n.d.
F_0	**Pb^{2+} dark**		**Pb^{2+} 25PAR**		**Pb^{2+} 65PAR**	
	log hEC	log EC50	log hEC	log EC50	log hEC	log EC50
acute	-4.00	-1.374	-4.00	-1.374	-4.00	-1.212
24h	-4.00	-1.333	-4.00	-1.359	-4.00	-1.293
48h	-4.00	-1.293	-4.00	-1.345	-4.00	-1.343
week	-4.00	n.d.	-4.00	n.d.	-4.00	n.d.
rec	-4.00	n.d.	-4.00	n.d.	-4.00	n.d.

419

3.5. Visual inspection at optical microscope

The main species dominating the river biofilm colonising the glass slides were green algae: *Trentepohlia aurea* and *Trentepohlia* sp., *Printzina* sp., *Chlorochytrium* sp., *Klebsormidium flaccidum*, *Stigeoclonium tenue*, *Mougeotia* sp., *Trebouxia* sp., *Oedogonium* sp.; diatoms were present on top of green algae, in particular, the species: *Achnanthidium* sp., and in less extent *Synedra* sp. and *Gomphonema* sp. The proportion of diatoms and chlorophyceae in the slides was about the same with a slight prevalence of chlorophyceae (3.28 x 10^ 7 org/cm2 chlorophyceae and 4.17 x 10^4 org/cm2 diatoms). Biofilms were analysed by optical confocal and stereoscopic microscopy again after the experiment, i.e. after the recovery period. Some selected samples are shown in Figure 9: control biofilm showed diatoms growing on top of green algae forming multiple layers and a thick coverage, biofilm exposed to Cu1mM showed some necrosis, especially evident in the filamentous green algae; at very high doses the high amount of Cu incorporated by green algae caould be visualised by its light blue colour (Fig. 9). Sample exposed to high Zn concentration lost the green spots that represent green algae (Fig. 9). In Figures 10, 11, 12 are shown selected images at bigger magnification of examples of several main species colonising the slides.

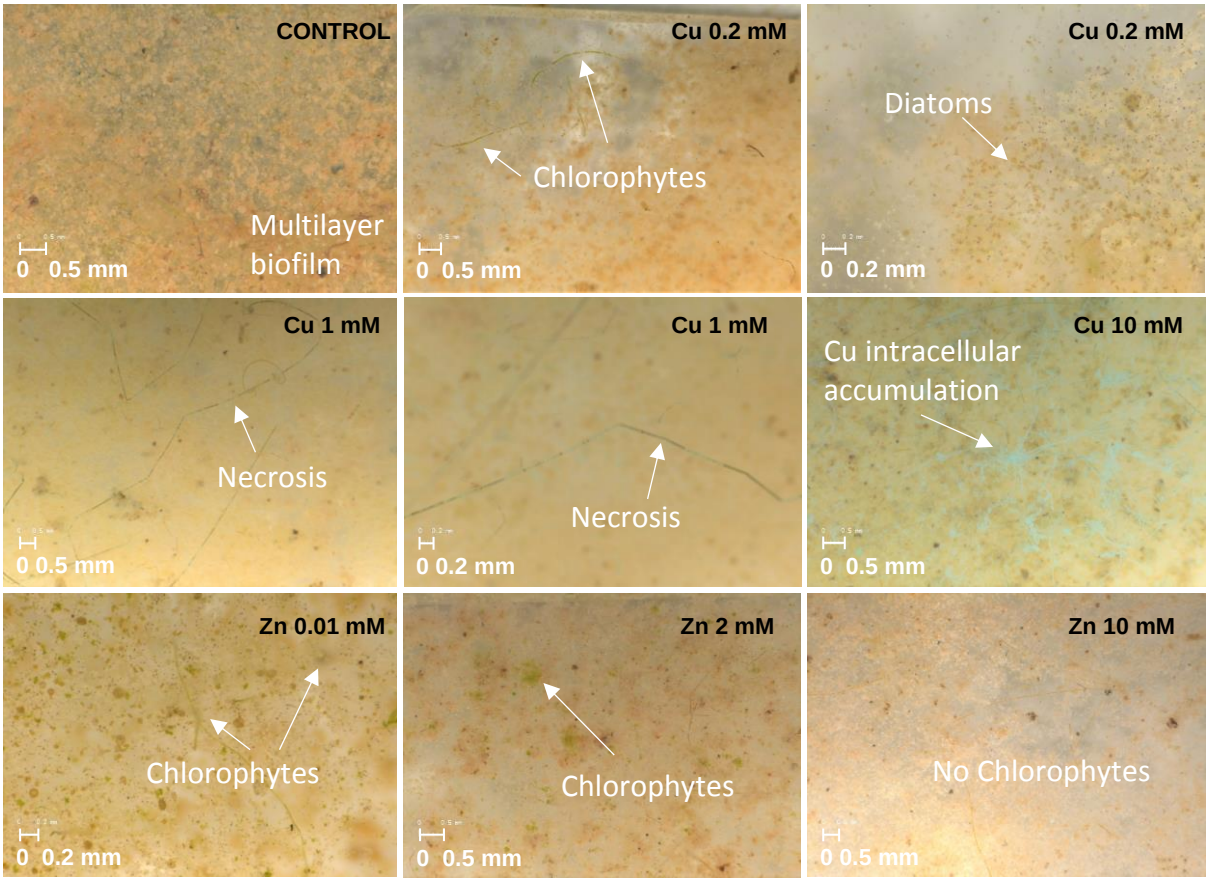

436

437 Figure 9. Pictures of selected biofilms at stereoscopic microscope after the recovery period.

438 Exposure concentrations are indicated on the upper right.

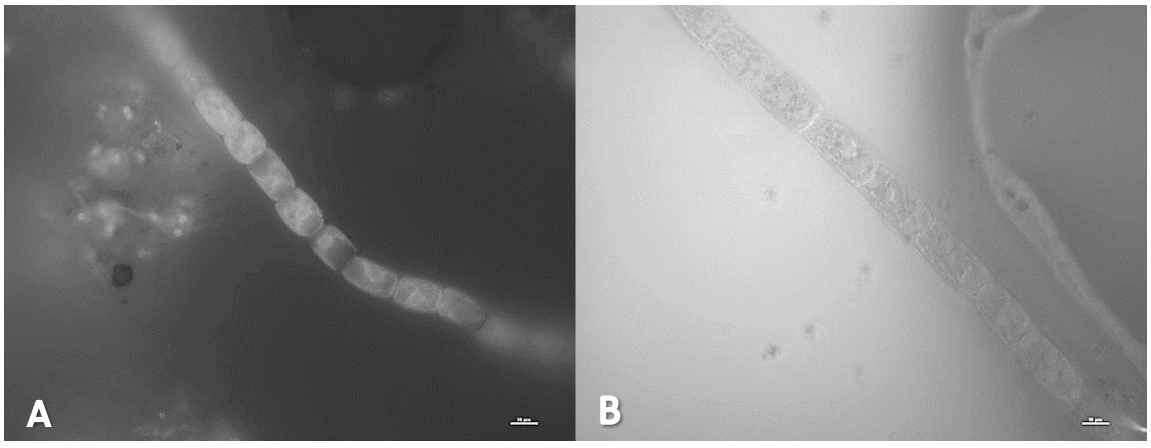

439

440 Figure 10. Confocal images of filamentous Chlorophytes from biofilm sample. A: 400X, 633

441 nm. B: 400X, 543 nm.

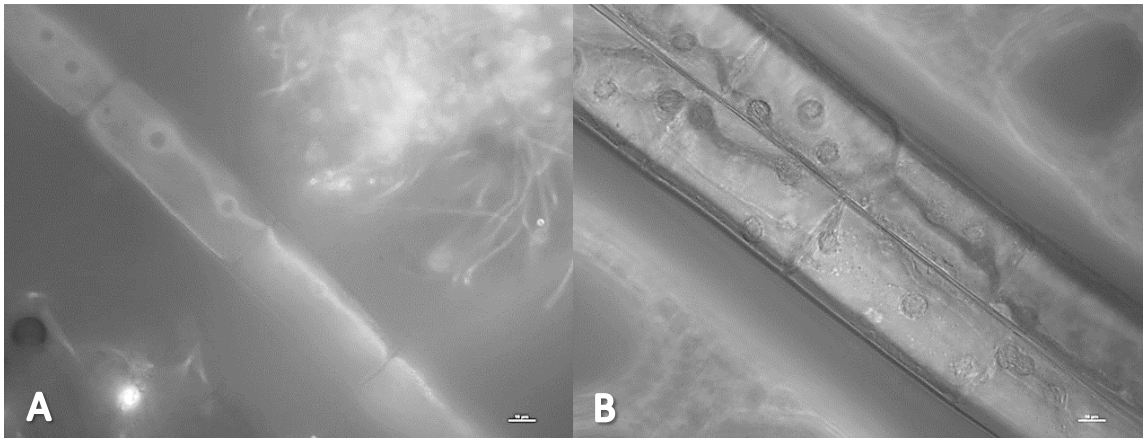

Figure 11. Confocal images of filamentous Chlorophytes: *Mougeotia* sp. from biofilm sample. A: 400X, 543 nm. B: 500X, 543 nm.

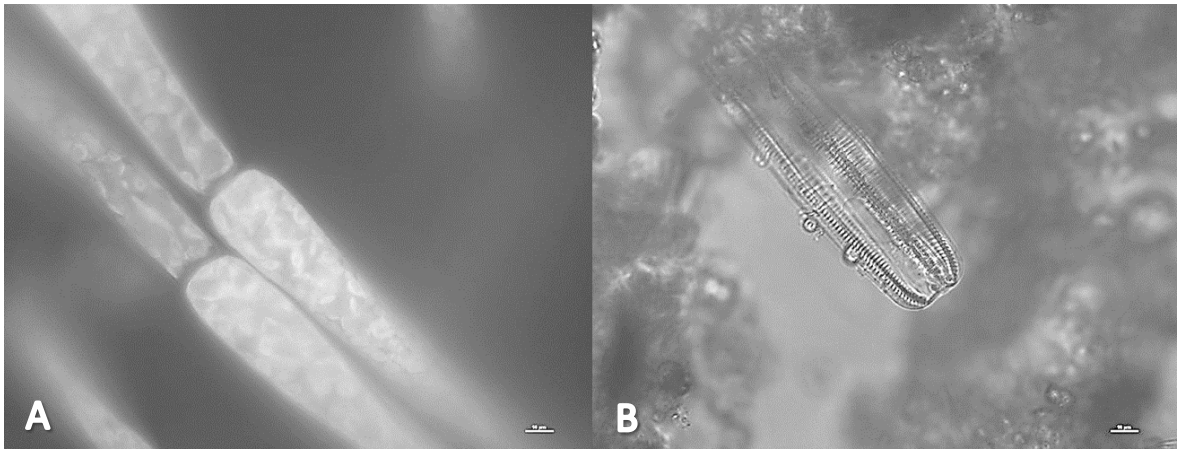

Figure 12. Confocal images of filamentous Chlorophytes and Bacillariophyceae from biofilm samples. A: 400 X, 633nm, *Oedogonium* sp. B: 400X, white light, Diatom.

3.6. Discussion

The micro-PAM sensor used in this study is tailored to field measurements due to its compact measuring head, its waterproof housing, its low energy demand and has a restrained price respect to more complex PAM such as IMAGING-PAM. The performed tests in laboratory were useful to verify the performance of this sensor in controlled conditions: micro-PAM shows the same level of sensibility of bigger PAM instruments such as IMAGING-PAM and PHYTO-PAM, the results of this comparison will be presented elsewhere (Carafa et al., *in*

preparation). Micro-PAM is suited in particular for small samples and its use on river biofilm is appropriate. A laboratory calibration it is recommended before the use in field in order to adjust settings and verify the most interesting functional parameters to record. Taking into account the use of this sensor inside a monitoring device including a 'local reference' the variability of the biofilm response can be considered in a relative way instead than in an absolute way and it is justified to use a more sensitive local upstream biofilm to obtain a preliminary calibration of the sensor and to select interesting parameters to record.

In this study the tests were performed using BBM medium containing EDTA: the effect of EDTA on heavy metal toxicity is heavy metal- and EDTA concentration-dependent. Our results indicate that it is preferable to calculate the bioavailable percentage of heavy metals, as the binding effect of EDTA should not be overlooked. Nevertheless, he speciation and metal binding does not explain alone the different metal toxicity, for example As was not complexed with EDTA but showed lower toxicity; other chemical and biological interaction play an important role in the final toxicity.

Toxicity values of the three parameters considered in this study (YII, NPQ, and F_0) appear similar in the order of magnitude but give complimentary information if we look at the different curve fitting. The mechanisms that are involved in HMs toxicity on photosynthesis are very complex and still a matter of speculation, but different authors agreed that involve electron transport in light reactions and enzyme activity in the dark reactions (Kycko et al., 2019). This induced toxic stress together with the protective responses of cell metabolism can give an explanation of the behaviour of the NPQ in our tests. According to our results NPQ, in fact, is the parameter that reacts more quickly: is stimulated during low and acute toxicity, and starts to be depressed when the cells are no longer able to detoxify. Some authors, in accordance with our results, found a decrease of the NPQ in microcosm experiments after long-term exposures of Zn (Corcoll et al., 2011). YII is the most used parameter in PAM fluorometry and our results

are comparable with several studies in the literature. Corcoll et al. (2012) and Bradac et al., (2009) observed that, after few hours of exposure, metal toxicity measured as a decrease in YII, is more related to metal bioaccumulation than to metal concentration in water, this can explain the delay in the observation of the response. F_0 and F_0'are in general not considered in toxicity tests. In our study F_0 after chronic exposure seems very robust with the advantage to be easier to measure. Xu et al. (2016) found significant differences in the photosynthetic quantum yields following exposure to 3.89 and 7.85 mg/L Zn^{2+} for 6 h, and after 21 days' exposure noticeable community composition changes (i.e., substantial loss of diatoms). The steep concentration-response curve for Zn exposed sample that we observed in our study could be explained taking into account both bioaccumulation processes and the mode of action of Zn, targeting several photosynthetic processes of algae, diatoms and cyanobacteria (Admiraal et al., 1999). Long term effects on diatoms by Zn were also registered by Ivorra et al. (2002).

In the metabolism of photosynthetic organisms, Cu can show opposite effects: it is an essential micronutrient but at higher concentrations (>100 µg L^{-1}) or long exposure time may become toxic (Serra et al., 2009). Chronic exposure to Cu is known to result in structural and functional effects in autotrophic and heterotrophic biofilm microbial communities (Soldo and Behra, 2000; Boivin et al., 2006; Serra and Guasch, 2009; Serra et al., 2009; Maksymiec, 1997). Guash et al. (2002), found that Cu exposure of periphyton of oligotrophic calcareous rivers at 10–20 µg/L (12 days of exposure) caused stronger effects on structural (algal biomass and community structure) than on functional (photosynthetic efficiency) parameters of periphyton. Exposure to Cu for 96 h induced significant growth differences in the diatom *Tabellaria flocculosa* at 6 and 10 µg/L, with approximately 50% and 70% growth inhibition, respectively and increase in oxidative stress (Gonçalves et al., 2018). These studies could justify the use of basal fluorescence, which is correlated with algal biomass, as an endpoint after chronic HMs exposure and confirm in part our data. However, we measured a decrease of F_0 also after short

505 time exposure (24h), more modelling studies taking into account algal physiology are needed
506 to better understand the behaviour of this parameter. Acute toxicity effects of As were observed
507 on the photosynthetic efficiency of diatoms and cyanobacteria whereas green algae were less
508 affected (Tuulaikhuu et al., 2015; Rodriguez Castro et al. 2014). Other As effects observed in
509 river biofilms include growth reduction, less nitrogen content, higher dead diatom densities
510 and a decrease in phototrophic component (Barral-Fraga et al., 2018). Exposure to an
511 environmentally realistic concentration of As (120 μgL^{-1}) in an in indoor experimental channels
512 mimicking a fluvial system caused these effects: lowering the total biomass of biofilm and its
513 potential ability to use organic P (i.e., phosphatase activity), inhibiting algal growth, especially
514 that of diatoms, decreasing nitrogen content, and making the epipsammic biofilm more
515 heterotrophic, thus reducing its ability to oxygenate the aquatic environment (Tuulaikhuu et
516 al., 2015). The toxicity we measured for As was very low respect to the other HMs (except
517 Pb). Taking into account the listed previous studies, probably the justification of our results is
518 linked to the specific species sensitivity in our biofilms. Lawrence et al. (2004) found that some
519 effects of Ni in biofilms were the elimination of cyanobacterial populations and reduced
520 photosynthetic biomass in the biofilms. In the same study, Ni at 0.5 mg/L resulted in reductions
521 in carbon utilization; the presence of Ni eliminated the positive influence of nutrients on the
522 biofilms. This study is in agreement with our results indicating a reduction of F_0 after Ni
523 chronic exposure. The green microalgae *A. falcatus* is highly sensitive to Ni concentrations as
524 low as 1 $\mu g\ L^{-1}$: photosynthetic pigments are reduced and Ni^{2+} increases antioxidant enzyme
525 responses (Martínez-Ruiz and Martínez-Jerónimo, 2015). In our study EC50 of Ni (about 1
526 mg/L) is higher of the values found in the literature for single species but it is in accordance
527 with the study of Lawrence et al. (2004) in biofilms. For Pb, de Oliveira Gonçalves Alho et al.
528 (2019) found an IC50–72 h of 0.78 μM and measured significant changes of chlorophyll-a
529 synthesis and a reduction of both efficiencies of oxygen-evolving complex and quantum yields.

In our study, Pb does not affect biofilms, but for this metal the sequestration rate by EDTA was important: in this case, it would be probably better to perform the test in a modified medium with lower or no EDTA. However, in this case, the effects of lack of EDTA have to be also considered, to avoid biased results. Mineralization of Lead on EPS produced by cells in biofilms may occur in natural environments and was assessed in the laboratory by Couasnon et al. (2019). In the case of Zn and As exposure, a recovery in biofilm functional parameters is observed after one week in a clean medium in this study. Lambert et al. (2012) found that changes in biofilm microbial communities generally lead to an increase in community tolerance to metals, in line with the concept introduced by Blanck et al. (1988). Anyway, these changes take time to produce a complete recovery. Lambert et al. (2012) measured 6 weeks for a complete recovery after Cu exposure in river biofilm and only when was possible an immigration process in the presence of pristine not affected communities. Corcoll et al. (2012) measured recovery from Zn exposure after 3 to 5 weeks; this recovery was also explained by changes in the community composition. In our case no external colonization was possible, and the recovery was due mainly to cell detoxification processes.

Effects on changes in the community and possible adaptation can appear in the field, this community shift may affect the sensitivity of the biofilms and of the tested sensor in detecting acute contamination events: more experiments in filed are needed to evaluate the magnitude of this possible adaptation. More research is needed in order to evaluate the sensitivity and the temporal variability in field of the micro-PAM sensor and the associated monitoring device, but this study represents a first calibration step. Based on laboratory results it seems better to use high PAR intensities, close to saturation, in order to obtain more fast and clear results, and it is recommended to measure at least YII, NPQ because are complementary parameters giving information respectively on chronic and acute effects.

4. Conclusions

Early effects of HMs affect river biofilm functions, supporting the use of Chla fluorescence techniques as signals of early toxicity. In particular, in this study the survey of two parameters which are very easy to measure as indicators of possible contamination events, are suggested additionally to the YII, traditionally used to assess effects of metals on the photosystem: basal fluorescence F_0 and non-photochemical quenching NPQ. The suitability of the new micro-PAM sensor to assess early effects of zinc, copper, nickel, arsenic, and lead in river biofilms, was shown by our results: stimulation of NPQ is a clear acute effect, especially in illuminated samples, while depression of YII and F_0 is evident especially in chronic tests. NPQ shows a clear hormetic behaviour in chronic tests with a narrow threshold between max stimulation and EC100. The next steps to validate this sensor and the associated monitoring device will be to test its sensitivity compared with other PAM instruments, to assess the sensitivity of the biofilm community to pharmaceuticals and pesticides, to calibrate in the field in selected rivers and WWTP outflows and to assess mixture effects. Chla fluorescence in biofilm as a warning system is particularly indicated for short term pollution detection, suggesting this parameter may be useful for detecting recent contamination and in online monitoring. A further improvement of the sensor will be the implementation of measurements at a different wavelength that will allow the detection of effects more specifically in diatoms and cyanobacteria. This study, as a first step in the calibration of an in-continuous monitoring device, is of interest for their possible application in EU monitoring programs. Nevertheless, more research is needed to test the microsensor in the field and validate the results obtained in laboratory assays.

Acknowledgements

The authors thank the Tecniospring Plus programme and ACCIÓ for funding this project. This project has received funding from the European Union's Horizon 2020 research and innovation

programme under the Marie Skłodowska-Curie grant agreement No 712949. Xavier Gomara Barbera from URV, supported part of the laboratory analysis. V. Kumar received funds from Health Department of Catalonia Government trough "Pla Estratègic de Recerca i Innovació en salut" (PERIS 2016-2020).

References

Admiraal W, Blanck H, Jong M, Guasch H, Ivorra N, Lehmann V, Nyström BAH, Paulsson M, Sabater S, 1999. Short-term toxicity of zinc to microbenthic algae and bacteria in a metal polluted stream. Water Research 33, 1989-1996.

Aro EM, Suorsa M, Rokka A, Allahverdiyeva Y, Paakkarinen V, Saleem A, Battchikova N, Rintamäki E, 2005. Dynamics of photosystem II: A proteomic approach to thylakoid protein complexes. Journal of Experimental Botany 56, 347-356.

Baker NR, 2008. Chlorophyll fluorescence: a probe of photosynthesis in vivo. Annual Review of Plant Biology 59, 89-113. https://doi.org/10.1146/annurev.arplant.59.032607.092759.

Barral-Fraga L, Martiñá-Prieto D, Barral MT, Morinc S, Guasch H, 2018. Mutual interaction between arsenic and biofilm in a mining impacted river. Science of the Total Environment 636, 985–998.

Battin TJ, Kaplan LA, Newbold JD, Hansen CME, 2003. Contributions of microbial biofilms to ecosystem processes in stream mesocosms. Nature 426,439-441.

Bellinger E G and Sigee D C, 2010. Freshwater Algae: Identification and Use as Bioindicators John Wiley & Sons, Ltd 118 pp.

Bilger W, Björkman O, 1990. Role of the xanthophyll cycle in photoprotection elucidated by measurements of light-induced absorbance changes, fluorescence and photosynthesis in leaves of *Hedera canariensis*. Photosynthesis Research 25, 173-185.

602 Blanck H, Wängberg, SA, Molander S, 1988. Pollution-induced community tolerance – a new
603 ecotoxicological tool. In: Cairns, J., Pratt, J.R. (Eds.), Functional. Testing of Aquatic Biota for
604 Estimating Hazards of Chemicals, pp. 219-230, Philadelphia, ASTM STP 988.

605 Boisvert S, Joly D, Leclere S, Govindachary S, Harnois J, Carpentier R, 2007. Inhibition of the
606 oxygen-evolving complex of photosystem II and depletion of extrinsic polypeptides by nickel.
607 Biometals 20, 879-889.

608 Boivin MEY, Massieux B, Breure AM, Greve GD, Rutgers M, Admiraal W, 2006. Functional
609 recovery of biofilm bacterial communities after copper exposure. Environmental Pollution 140,
610 239-246.

611 Bonet B, Corcoll N, Guasch H, 2012. Antioxidant enzyme activities as biomarkers of Zn
612 pollution in fluvial biofilms. Ecotoxicology and Environmental Safety 80, 172-178.

613 Bradac P, Navarro E, Odzak N, Behra R, Sigg L, 2009. Kinetics of cadmium accumulation in
614 periphyton under freshwater conditions. Environ. Toxicol. Chem. 28, 2108–2116.

615 Carafa R., Gallé T., Sierra Llopart J., Vázquez Vilamajó L., 2020. Dispositivo de
616 monitorización de sustancias tóxicas en agua y sistema que lo comprende. Solicitud de Patente
617 Nacional en España Nº 202030285. S/Ref.: N/Ref.: 2019/51535.

618 Cemagref, 1982. Etude des Methodes Biologiques d'Appreciation Quantitative de la Qualité
619 des Eaux. Rapport Q.E. Lyon, Agence de 'Eau Rhone-Mediterranée-Corse –Cemagref, Lyon,
620 France.

621 Corcoll N, Bonet B, Leira M, Guasch H, 2011. Chl-a fluorescence parameters as biomarkers
622 of metal toxicity in fluvial biofilms: an experimental study. Hydrobiologia 673, 119-136.

623 Corcoll N, Bonet B, Morin S, Tlili A, Leira M, Guasch H, 2012. The effect of metals on
624 photosynthesis processes and diatom metrics of biofilm from a metal-contaminated river: A
625 translocation experiment. Ecological Indicators 18, 620-631.

626 Corcoll N, Casellas M, Huerta B, Guasch H, Acuña V, Rodríguez-Mozaz S, Serra-Compte A,
627 Barceló D, Sabater S, 2014. Effects of flow intermittency and pharmaceutical exposure on the
628 structure and metabolism of stream biofilms. Science of the Total Environment, 15, 503-504,
629 159-70. doi: 10.1016/j.scitotenv.2014.06.093.

630 Couasnon T, Gélabert A, Ona-Nguema G, Zanna S, Ménez B, Guyot F, 2019. Experimental
631 assessment of occurrences and stability of lead-bearingminerals in bacterial biofilms. Chemical
632 Geology 505, 23-35.

633 Demmig-Adams, B., Garab, G., Adams III, W.W., Govindjee (Eds.), 2014. Non-
634 photochemical quenching and energy dissipation in plants, algae and cyanobacteria. Advances
635 in Photosynthesis and Respiration. pp. 40. Springer Science+Business Media Dordrecht.

636 de Oliveira Gonçalves Alho L, Castelhano Gebara R, de Araujo Paina K, Sarmento H, da Graça
637 Gama Melão M, 2019. Responses of *Raphidocelis subcapitata* exposed to Cd and Pb:
638 Mechanisms of toxicity assessed by multiple endpoints. Ecotoxicology and Environmental
639 Safety 169, 950-959.

640 de Sostoa A., Caiola N., Casals F., García-Berthou E., Alcaraz C., Benejam L., Maceda A.,
641 Solà C., Munné A., 2010. Ajust de l'Índex d'Integritat Biòtica (IBICAT) basat en l'ús dels
642 peixos com a indicadors de la qualitat ambiental als rius de Catalunya.
643 10.13140/2.1.1551.6964.

644 Eggert A, Häubner N, Klausch S, Karsten U, Schumann R, 2006. Quantification of algal
645 biofilms colonising building materials: chlorophyll a measured by PAM-fluorometry as a
646 biomass parameter. Biofouling, 22,2, 79-90. DOI: 10.1080/08927010600579090

Gonçalves S, Kahlert M, Almeida SF, Figueira E, 2018. Assessing Cu impacts on freshwater diatoms: biochemical and metabolomic responses of *Tabellaria flocculosa* (Roth) Kützing. Science of the Total Environment. 625, 1, 1234-1246.

Guasch H, Paulsson M, Sabater S, 2002. Effect of copper on algal communities from oligotrophic calcareous streams. Journal of Phycology 38, 241-248.

Guasch, H., Admiraal, W., Sabater, S., 2003. Contrasting effects of organic and inorganic toxicants on freshwater periphyton. Aquat. Toxicol. 64, 165–175.

Gustafsson, J. P. 2014. "Visual MINTEQ 3. 1 User Guide," 1–73.

Handa S, Frisch A and OhmuraY, 2014. Morphology of Trentepohlialean Photobionts Isolated from Arthoniales of the Imperial Palace Grounds, Tokyo, Japan. Mem. Natl. Mus. Nat. Sci., Tokyo, 49, 219–226.

Hawkes, H.A (1998). Origin and development of the biological monitoring working party score system. Water Research. 32 (3): 964–968.

Ivorra N, Barranguet C, Jonker M, Kraak MHS, Admiraal W, 2002 Metal-induced tolerance in the freshwater microbenthic diatom *Gomphonema parvulum*. Environmental Pollution 116, 147-157.

John D M, Whitton B A, Brook A J (Editors), 2002. The Freshwater Algal Flora of the British Isles An Identification Guide to Freshwater and Terrestrial Algae Field / Identification Guide Identification Key. 878 pp.

Kumar KS, Dahms H-U, Lee J-S, Kim HC, Lee WC, Shin K-H, 2014. Algal photosynthetic responses to toxic metals and herbicides assessed by chlorophyll a fluorescence. Ecotoxicology and Environmental Safety 104, 51-71. https://doi.org/10.1016/j.ecoenv.2014.01.042.

669 Kycko M, Romanowska E, Romanowska, Zagajewski B, 2019. Lead-Induced Changes in
670 Fluorescence and Spectral Characteristics of Pea Leaves. Remote Sensing 11, 16, 1885. DOI:
671 10.3390/rs11161885.

672 Lambert A-S, Morin S, Artigas J, Volat B, Coquery M, Neyra M, Pesce S, 2012. Structural and
673 functional recovery of microbial biofilms after a decrease in copper exposure: Influence of the
674 presence of pristine communities. Aquatic Toxicology 109, 118-126.

675 Lavoie M, Raven JA, Jones OAH, Qiane H, 2016. Energy cost of intracellular metal and
676 metalloid detoxification in wild-type eukaryotic phytoplankton. Metallomics, 8, 1097-1109.
677 DOI: 10.1039/C6MT00049E.

678 Lawrence JR, Chenier MR, Roy R, Beaumier D, Fortin N, Swerhone GDW, Neu TR, Greer
679 CW, 2004. Microscale and molecular assessment of impacts of nickel, nutrients, and oxygen
680 level on structure and function of river biofilm communities. Applied and environmental
681 microbiology 70, 7, 4326-4339.

682 Lawson J., 2005. River Basin Management. Progress Towards Implementation of the European
683 Water Framework Directive. ISBN 9780415392006. Book Published by CRC Press. 396 pp.

684 Leguay S, Lavoie I, Levy JL, Fortin C, 2016. Using biofilms for monitoring metal
685 contamination in lotic ecosystems: The protective effects of hardness and pH on metal
686 bioaccumulation. Environmental Toxicology and Chemistry 35, 6, 1489-501. doi:
687 10.1002/etc.3292.

688 Maksymiec W, 1997. Effect of copper on cellular processes in higher plants. Photosynthetica
689 34, 321-342.

690 Martínez-Ruiz EB, Martínez-Jerónimo F, 2015. Nickel has biochemical, physiological, and
691 structural effects on the green microalga *Ankistrodesmus falcatus*: an integrative study. Aquatic
692 Toxicology 169, 27-36.

693 Maxwell K, Johnson GN. 2000. Chlorophyll Fluorescence--a Practical Guide. Journal of
694 Experimental Botany 51, 345, 659–68. doi:10.1093/jexbot/51.345.659.

695 Margoum C, Morin S, Mazzella N, 2015. Potential toxicity of pesticides in freshwater
696 environments: Passive sampling, exposure and impacts on biofilms: the PoToMAC project.
697 Environmental Science and Pollution Research 22, 3985-3987.
698 https://doi.org/10.1007/s11356-014-3291-z.

699 Miles CD, Brandle JR, Daniel DJ, Chu-Der O, Schnare PD, Uhlik, DJ, 1972. Inhibition of
700 photosystem ii in isolated chloroplasts by lead. Plant physiology 49, 820–82.

701 Mykhaylenko NF, Zolotareva EK, 2017. The Effect of Copper and Selenium Nanocarboxylates
702 on Biomass Accumulation and Photosynthetic Energy Transduction Efficiency of the Green
703 Algae Chlorella Vulgaris. Nanoscale Res Lett. 12(1):147.

704 Muyssen BTA, Brix KV, De Forest DK, Janssen CR, 2004. Nickel essentiality and homeostasis
705 in aquatic organisms. Environmental Reviews 12, 113-131.

706 Nichols H and Bold H, 1965. Growth media-Fresh water. In: Stein JR (Ed.), Hand Book of
707 Physiological. Methods, Cambridge University Press, Cambridge. pp. 7-24.

708 Nõges P, Argillier C, Borja Á, Garmendia JM, Hanganu J, Kodeš V, Pletterbauer F, Sagouis
709 A, Birk S, 2016. Quantified biotic and abiotic responses to multiple stress in freshwater, marine
710 and ground waters. Science of the Total Environment 2016 1, 540, 43-52. doi:
711 10.1016/j.scitotenv.2015.06.045.

712 Pesce S, Bardot C, Lehours AC, Batisson I, Bohatier J, Fajon C, 2008. Effects of diuron in
713 microcosms on natural riverine bacterial community composition: new insight into
714 phylogenetic approaches using PCR-TTGE analysis. Aquatic Sciences 70, 410-418.

715 Pesce S, Lissalde S, Lavieille D, Margoum C, Mazzella N, Roubeix V, Montuelle B, 2010.
716 Evaluation of single and joint toxic effects of diuron and its main metabolites on natural
717 phototrophic biofilms using a pollution-induced community tolerance (PICT) approach.
718 Aquatic Toxicology, 99, 4, 492-499.

719 Pessarakli M, 2016. Handbook of Photosynthesis - 3rd Edition CRC Press. pp. 846. ISBN
720 9781482230734.

721 Pinto J, Sigaud-Kutner, TCS, Leitão MAS, Okamoto OK, Morse D, Colepicolo P, 2003. Heavy
722 metal-induced oxidative stress in algae. Journal of Phycology 39, 1008-1018.

723 Poonkothai M, Vijayavathi BS, 2012. Nickel as an essential element and a toxicant.
724 International Journal of Engineering Science 1, 4, 285-288.

725 Proia L, Morin S, Peipoch M, Romaní AM, Sabater S, 2011. Resistance and recovery of river
726 biofilms receiving short pulses of triclosan and diuron. Science of the Total Environment 409,
727 3129-3137. http://dx.doi.org/10.1016/j.scitotenv.2011.05.013.

728 Proia L, Vilches C, Boninneau C, Kantiani L, Farré M, Romaní AM, Sabater S,Guasch H,
729 2013. Drought episode modulates the response of river biofilms to triclosan. Aquatic
730 Toxicology 127, 36-45. http://dx.doi.org/10.1016/j.aquatox.2012.01.006.

731 Roca M, Martín-Vide JP, Moreta PJM, 2009. Modelling a torrential event in a river confluence.
732 Journal of Hydrology 364, 3-4, 207-215.

733 Rodriguez Castro MC, Urrea G, Guasch H, 2014. Influence of the interaction between
734 phosphate and arsenate on periphyton's growth and its nutrient uptake capacity. Science of the
735 Total Environment 503-504, 122-132. http://dx.doi.org/10.1016/j.scitotenv.2014.06.094.

736 Roig N, Sierra J, Nadal M, Moreno-Garrido I, Nieto E, Hampel M, Pérez-Gallego E,
737 Schuhmacher M, Blasco, J, 2015. Assessment of sediment ecotoxicological status as a
738 complementary tool for the evaluation of surface water quality. The Ebro river basin case study.
739 Science of the Total Environment 503-504, 269-278.
740 https://doi.org/10.1016/j.scitotenv.2014.06.125.

741 Roig N, Sierra J, Ortiz, J, Merseburger G, Schuhmacher M, Domingo JL, Nadal M, 2013.
742 Integrated study of metal behavior in Mediterranean stream ecosystems: A case study. Journal
743 of Hazardous Materials 263, 122-130. https://doi.org/10.1016/j.jhazmat.2013.07.051.

744 Sabater S, Guasch H, Ricart M, Romaní AM, Vidal G, Klünder C, Schmitt-Jansen M, 2007.
745 Monitoring the effect of chemicals on biological communities. The biofilm as an interface.
746 Analytical and Bioanalytical Chemistry 387, 1425-1434.

747 Schmitt-Jansen M, Altenburger R, 2008. Community-level microalgal toxicity assessment by
748 multiwavelength-excitation PAM fluorometry. Aquatic Toxicology 86, 49-58.

749 Schreiber U, Müller JF, Haugg A, Gademann R, 2002. New type of dual-channel PAM
750 chlorophyll fluorometer for highly sensitive water toxicity biotests. Photosynthesis Research
751 74, 317-330.

752 Schreiber U, 2004. Pulse-Amplitude-Modulation (PAM) fluorometry and saturation pulse
753 method: an overview. In: Chlorophyll a Fluorescence. Advances in Photosynthesis and
754 Respiration. Papageorgiou G.C., Govindjee (eds). 19, 279-319. Dordrecht Netherlands:
755 Springer.

Serra A, Corcoll N, Guasch H, 2009. Copper bioaccumulation and toxicity in fluvial periphyton: the influence of exposure history. Chemosphere 74, 633-664.

Serra A, Guasch H, 2009. Effects of chronic copper exposure on fluvial systems: linking structural and physiological changes on fluvial biofilms with the instream copper retention. Science of the Total Environment 407, 5274-5282.

Serra A, Guasch H, Admiraal W, Van der Geest HG, Van Beusekom SAM, 2010. Influence of phosphorus on copper sensitivity of fluvial periphyton: the role of chemical, physiological and community-related factors. Ecotoxicology 19, 770-780.

Soldo D, Behra R, 2000. Long-term effects of copper on the structure of freshwater periphyton communities and their tolerance to copper, zinc, nickel and silver. Aquatic Toxicology 47, 181-189.

Tiam SK, Morin S, Bonet B, Guasch H, Feurtet-Mazel A, Eon M, Gonzalez P, Mazzella N, 2015. Is the toxicity of pesticide mixtures on river biofilm accounted for solely by the major compounds identified? Environmental Science and Pollution Research 22, 6, 4009-4024.

Tuulaikhuu B-A, Romaní AM, Guasch H, 2015. Arsenic toxicity effects on microbial communities and nutrient cycling in indoor experimental channels mimicking a fluvial system. Aquatic Toxicology 166, 72-82.

Xu Y, Wang C, Hou J, Dai S, Wang P, Miao L, Lv B, Yang Y, You G, 2016. Effects of ZnO nanoparticles and Zn2+ on fluvial biofilms and the related toxicity mechanisms. Science of the Total Environment 544, 230-237.

Yoshimasu T, Ohashi T, Oura S, Kokawa Y, Kawago M, Hirai Y, Miyasaka M, Nishiguchi H, Kawashiman S, Yata Y, Honda M, Fujimoto T, Okamura Y, 2015. A Theoretical Model for

778 the Hormetic Dose-response Curve for Anticancer Agents. Anticancer Research 35, 11, 5851-
779 5855.

780 Zvezdanović J, Marković D, 2009. Copper, iron, and zinc interactions with chlorophyll in
781 extracts of photosynthetic pigments studied by VIS spectroscopy. Russian Journal of Physical
782 Chemistry A 83, 9, 1542-1546.

Figures and tables captions

Figure 1. Positioning of the glass slides for biofilm colonization in the Brugent River (a) and glass slides after biofilm colonization (b).

Figure 2. Configuration of laboratory tests: river biofilm on a glass slide (black numbered grill below) and the two micro PAM sensors.

Figure 3. Metal speciation at the different treatment concentrations expressed as % of total metal concentration. Not bioavailable species are indicated with grey shades and bioavailable species with colours. For As only two species present were at equal concentrations for all treatments.

Figure 4. NPQ concentration-response curves (lines) and experimental data (o) for Zinc and Copper exposed samples. Exponential model y = a*exp(b*x) + c*exp(d*x), DFE: 14. Hormetic model y = ((a- b)./(1+(exp((c* x)-d)))./(1+(exp((e*x)- f))). DFE: 12. Fit parameters in Matlab: MaxFunEvals = 6000; MaxIter = 40000; Robust = 'Bisquare'.

Figure 5. NPQ concentration-response curves (lines) and experimental data (o) for Nickel and Arsenic exposed samples. Exponential model y = a*exp(b*x) + c*exp(d*x), DFE: 14. Hormetic model y = ((a- b)./(1+(exp((c* x)-d)))./(1+(exp((e*x)- f))). DFE: 12. Fit parameters in Matlab: MaxFunEvals = 6000; MaxIter = 40000; Robust = 'Bisquare'.

Figure 6. NPQ concentration-response curves (lines) and experimental data (o) for Lead exposed samples. Exponential model y = a*exp(b*x) + c*exp(d*x), (DFE: 8). MaxFunEvals = 6000; MaxIter = 40000; Robust = 'Bisquare'.

Figure 7. YII concentration-response curves (lines) and experimental data (o) for Zn, Cu, Ni, As and Pb exposed samples. Hormetic model y = ((a- b)./(1+(exp((c* x)-d)))./(1+(exp((e*x)-f))). DFE: 12 (DFE 6 for Pb). Fit parameters in Matlab: MaxFunEvals = 6000; MaxIter = 40000; Robust = 'Bisquare'.

Figure 8. F_0 concentration-response curves (lines) and experimental data (o) for Zn, Cu, Ni, As and Pb exposed samples. Hormetic model y = ((a- b)./(1+(exp((c* x)-d)))./(1+(exp((e*x)- f))). DFE: 12 (DFE: 6 for Pb). Fit parameters in Matlab: MaxFunEvals = 6000; MaxIter = 40000; Robust = 'Bisquare'.

Figure 9. Pictures of selected biofilms at stereoscopic microscope after the recovery period. Exposure concentrations are indicated on the upper right.

Figure 10. Confocal images of filamentous Chlorophytes from biofilm sample. A: 400X, 633 nm. B: 400X, 543 nm.

Table 1. Tested single heavy metal dilutions (nominal concentrations in µg L^{-1} and corresponding concentration expressed in mM).

Table 2. The log maximum stimulated concentration (hEC) and the log half-maximal effective concentration (EC50, ppb) of NPQ for Zn, Cu and Ni on pristine river biofilms. * indicate an exponential fit curve.

Table 3. The log maximum stimulated concentration (hEC) and the log half-maximal effective concentration (EC50, ppb) of YII for Zn, Cu, Ni, As and Pb on pristine river biofilms.

Table 4. The log maximum stimulated concentration (hEC) and the log half-maximal effective concentration (EC50, ppb) of F_0 for Zn, Cu, Ni, As and Pb on pristine river biofilms.

Supplementary material

MICRO-PAM technical description.

General Design:

Housing:

Polymerhousing with optical block and fiber connector on one side a combined power line / RS485 socket on the opposite side.

Sample clip:

Consisting of 2 aluminum frames (3.5 x 2.5 cm), held together by magnet and mounted at a distance of 0.5 cm from the MONIHEAD/485 optical window. Angle between optical axis of the MONI-HEAD/485 and sample clip plane: 120°

Cables:

Data/power cable, 3 or 10 m standard length (between MICRO-PAM measuring head and interface box MICRO-PAM/I (for USB connection with Windows PC) or MONI-DA. Connected via M8 5-pin sealed connector

Dimensions:

Complete head with leaf clip: length 13,5 cm, 3.5 cm wide and 4 cm high

Power consumption**:**

Peak loads during saturating pulses 3 W. During measuring mode 0.15 W

Operating temperature**:** -15 to +40 °C

Weight: 96 g

Light Emission

Modulated fluorescence excitation**:**

Blue power LED (peak wavelength 465 nm, full width at half maximum 22 nm).

Photosynthetically active radiation (PAR) of measuring light at level of the sample

clip range from 0.15 to 1.5 µmol m-2 s-1 at low modulation frequencies (5 to 25 Hz), and from 1.5 to 22.5 µmol m-2 s-1 at high modulation frequencies (100 Hz)

Actinic light:

Same power LED as for modulated light. At level of sample clip, maximum photosynthetically active radiation of actinic light and saturating flashes 8000 µmol m-2 s-1. Actinic illumination can be chosen up to 3000 µmol m-2 s-1.

Sensors

Fluorescence:

PIN-photodiode protected by longpass filter (50% transmittance at 645 nm). Selective window amplifier to measure pulse amplitude modulated (PAM) fluorescence

Photosynthetically active radiation (PAR):

LS-C sensor for selective PAR measurement, range 0 to 7000 µmol m-2 s-1, cosine-corrected for light incident at angles between -30 ° to +30 from surface normal

Temperature:

Integrated-circuit temperature sensor on circuit board.

Leaf temperature thermocouple: Ni-CrNi, wire diameter 0.1 mm, -20 to +60 °C

Humidity:

Humidity and temperature sensing integrated circuit, 0 - 100% relative humidity.

Software:

WinControl-3 for PAM fluorometers. Measured and calculated parameters: Fo, Fm, Fm', F, Fo' (calculated), Fv/Fm (max. Yield), ΔF/Fm' (Yield), qP, qN, qL, NPQ, Y(NPQ), Y(NO), ETR (i.e. PAR x ΔF/Fm'), PAR and °C. Two different fitting routines for ETR versus light intensity curves

Computer Minimum Requirements

873 Processor, 1 GHz. RAM, 1 GB. Hard disc space, 1GB. Screen resolution, 800 x 600
874 pixels. Interface, USB 1.1/2.0/3.0, RS-232, or Ethernet. Operating system: Microsoft
875 Windows XP/Vista/7/8/10

Supplementary material Tables

Table 1. Physico-chemical characteristics of the river Brugent measured by Catalan Water Agency from 2015 to 2018 (average values, standard deviation and number of samples). Substances and parameters are in alphabetic order. * Indicates valued under detection limit, the detection limit is reported. The unit of measure are µg/L for all parameters except: pH- u.pH, Temperature -°C, water hardness - µg/L CaCO4, conductivity - µS/cm.

	Years								Years						
Substance or parameter	2015	2016	2017	2018	AVG	ST DEV	COUNT	Substance or parameter	2015	2016	2017	2018	AVG	ST DEV	COUNT
1,1,1-trichloroethane		0.5*					1	endosulfan II		0.002*					1
1,1,2,2-tetrachloroethane		1*					1	endosulfan sulfate		0.002*					1
1,1,2-trichloroethane		5*					1	endosulfane		0.003*					1
1,1-dichloroethane		6*					1	endrin		0.001*			0.001	0.00141	2
1,1-dichloroethene		5*					1	endrin ketone		0.002*					1
1,2,3-trichlorbenzene		0.5*					1	ethion		0.005*					1
1,2,4-trichlorobenzene		0.5*					1	ethyl azinfos		0.005*					1
1,2-dichlorobenzene		2*					1	ethylbenzene		2*					1
1,2-dichloroethane		6*					1	fluoranthene		0.005*					1
1,2-dichloropropane		4*					1	g-hexachlorocyclohexane		0.001*					1
1,3,5-trichlorobenzene		0.5*					1	heptachlor		0.001*					1
1,3-dichlorobenzene		2*					1	heptachloro epoxide A		0.002*					1
1,4-dichlorobenzene		2*					1	heptachloro epoxide B		0.002*			0.002	0.000	2
2,2',4,4',5,5'-hexabrominated diphenyl ether		0.001*					1	hexachlorobenzene		0.001*					1
2,2',4,4',5-pentabrominated diphenyl ether		0.001*					1	hexachlorobutadiene		0.5*					1
2,2',4,4'-tetrabrominated diphenyl ether		0.001*					1	hexachlorocyclohexane		0.001*					1
2,4'-DDD		0.002*					1	indeno(1,2,3-c,d)pyrene		0.002*					1
2,4'-DDE		0.002*					1	iron	28.833	29.833	39.167	37.333	32.974	20.072	78
2,4'-DDT		0.002*					1	isodrin		0.002*					1
4,4'- DDD		0.002*					1	lead	1.083	1.000	1.083	1.000	1.051	0.223	39
4,4'- DDE		0.002*					1	m(p)-xylene		2*					1
4,4'- DDT		0.002*					1	magnesium	33583	31167	32000	28000	31923	5546	39
4-n-nonylphenol		0.02*					1	malathion		0.005*					1
aclonifen		0.005*					1	manganese	3.917	2.000	3.833	2.000	3.154	3.98	39
a-hexachlorocyclohexane		0.001*					1	mercury		0.0005*					1
alachlor		0.002*					1	methyl parathion		0.005*					1
aldrin		0.002*					1	metolachlor		0.002*					1
aluminium	100.0	100.0	108.3	100.0	102.6	16.0	39	molinate		0.005*					1
ammonia	27.500	31.333	29.917	35.667	30.051	13.830	39	molybdenum	1.167	1.167	1.250	1.333	1.205	0.469	39
ammonium	216.7	250.0	225.0	200.0	228.2	109.9	39	monochlorobenzene		1*					1
anthracene		0.005*					1	naphthalene		5*					1
antimony	5.000	5.083	5.417	5.000	5.154	0.8124	39	nickel	1.000	1.000	1.583	2.667	1.308	0.766	39
arsenic	1.000	1.000	1.083	1.000	1.026	0.1601	39	nitrate	5000	5000	5400	5000	5123	444	13
atrazine		0.01*					1	nitrite	73	40	40	40	50	36.06	13
barium	64.167	61.500	73.083	64.667	66.128	16.232	39	nonylphenol		0.200			0.200		1
BDE-100		0.001*					1	orthophosphate	200	200	200	200	200	0.000	13
BDE-154		0.001*					1	oxadiazon		0.005*					1
BDE-28		0.001*					1	o-xylene		2*					1
benzene		2*					1	PAHs		0.000					1
benzo[a]pyrene		0.002*					1	Parathion		0.005*					1
benzo[b]fluoranthene		0.005*					1	pentachlorobenzene		0.001*					1
benzo[ghi]perylene		0.002*					1	pentachlorophenol		0.07*					1
benzo[k]fluoranthene		0.005*					1	pH	8.046	8.171	8.211	8.233	8.144	0.335	69
beryllium	5.000	5.000	5.417	5.000	5.128	0.8006	39	phenitrothion		0.005*					1
bicarbonats	233750	257000	253825	271000	249946	27732	13	potassium	1250	1750	1000	1000	1308	630	13
bifenox		0.004*					1	propazine		0.01*					1
boron	50.000	50.000	54.167	50.000	51.282	8.0064	39	Quinoxyfen		0.004*					1
bromodichloromethane		0.5*					1	selenium	0.608	0.558	3.158	1.567	1.451	1.450	39
bromoform		0.5*					1	simazine		0.01*					1
Butylated hydroxytoluene		10*					1	sodium	5250	5750	5000	5000	5308	630	13
cadmium	0.500	0.500	0.542	0.500	0.513	0.0801	39	strontium 90	1269	1025	1031	997	1100	358.03	39
calcium	89833	82583	83500	80667	84949	9470	39	sulfate	129750	127750	114500	117000	123462	23621	13
carbon tetrachloride		0.5*					1	temperature	13.917	12.500	12.600	9.000	12.703	5.249	37
chlorfenvinfos		0.000					1	terbutryne		0.01*					1
chloride	11350	10575	10000	10000	10592	1578	13	terbutylazine		0.01*					1
chlorine total	27.917	60.000	60.000	60.000	50.128	15.956	39	tetrachloroethylene		0.5*					1
chlorpyrifos		0.005*					1	TOC	1200	1550	1125	1000	1269	501	13
chrome	1.000	1.000	1.083	1.000	1.026	0.1601	39	t-octylphenol		0.01*					1
cis-1,2-dichloroethylene		4*					1	toluene		2*					1
cis-1,3-dichloropropene		2*					1	trans-1,2-dichloroethylene		6*					1
cobalt	25.000	25.000	27.083	25.000	25.641	3.9771	78	trans-1,3-dichloropropene		2*					1
conductivity	591	593	598	614	596	75.95	74	triallat		0.005*					1
copper	5.225	3.875	8.567	11.100	6.290	7.0657	39	trichloroethylene		0.5*					1
cybutryne		0.005*					1	trichlorofluoromethane		0.5*					1
cypermethrin		0.000					2	trichloromethane		0.5*					1
diazinon		0.005*					1	trifluralin		0.002*					1
dibromochloromethane		0.5*					1	vanadium	25.000	25.000	27.083	25.000	25.641	4.003	39
dichloromethane		5*					1	water hardness	395258	334558	323350	352300	358741	87334	29
dieldrin		0.002*					1	zinc	6.833	5.000	5.667	5.000	5.769	2.4221	39
endosulfan I		0.002*					1								

Table 2. Parameters and fit goodness coefficients of NPQ concentration-response curves for heavy metal exposed samples. Exponential model (x) = a*exp(b*x) + c*exp(d*x), (DFE: 14 for As, Cu, Ni, Zn; DFE: 8 for Pb). Coefficients 95% confidence bounds in parenthesis (only for exponential curves). Hormetic model (x) = ((a- b)./(1+(exp((c* x)-d)))./(1+(exp((e*x)-f))). DFE: 12. Fit parameters in Matlab: MaxFunEvals = 6000; MaxIter = 40000; Robust = 'Bisquare'.

Zn^{2+}			a	b	c	d	e	f	SSE	R^2	Adj R^2	RMSE
NPQ	acute	dark	0.194 (0.135, 0.245)	0.108 (-0.043, 0.213)	2.64e-05 (-0.0003, 0.0004)	1.666 (-0.557, 3.881)			0.074	0.848	0.815	0.073
		25 PAR	0.55 (0.35, 0.75)	0.01 (-0.19, 0.21)	0.004 (-0.025, 0.033)	0.985 (-0.278, 2.231)			0.443	0.830	0.793	0.178
		65 PAR	0.667 (0.150, 1.178)	-0.07 4 (-0.445 0.303)	0.058 (-0.176, 0.274)	0.634 (-0.067, 1.333)			0.911	0.839	0.805	0.255
	24h	dark	5.577	-4.961	3.222	18.220	-0.145	-3.845	0.231	0.362	0.096	0.139
		25 PAR	350.000	-39.010	6.617	35.070	-0.200	-6.788	1.008	0.625	0.469	0.290
		65 PAR	350.000	-39.020	5.257	27.750	-0.143	-6.235	1.135	0.684	0.552	0.308
	48h	dark	194.917	116.083	6.525	37.345	-0.169	-6.128	0.055	0.778	0.686	0.068
		25 PAR	1075.823	-875.823	4.860	26.631	-0.090	-7.981	0.585	0.578	0.402	0.221
		65 PAR	280.083	-80.088	4.660	25.143	-0.073	-5.925	2.333	0.141	-0.217	0.441
	week	dark	325.074	-1018.420	153.627	796.545	-0.003	-8.716	0.074	0.660	0.519	0.078
		25 PAR	1439.748	-1239.772	124.022	650.518	-0.044	-8.536	0.339	0.776	0.683	0.168
		65 PAR	2569.821	-3269.764	206.731	1083.262	-0.041	-9.011	0.535	0.783	0.693	0.211
	rec	dark	578.925	-1278.913	9.094	52.501	-0.033	-8.858	0.312	-0.393	-0.973	0.161
		25 PAR	253.661	-953.661	4.238	23.601	-0.075	-7.900	0.820	0.033	-0.370	0.261
		65 PAR	1200.168	-1900.168	4.080	22.427	-0.122	-8.518	1.585	0.320	0.036	0.364

Cu (except $CuHPO_4$ aq, $CuEDTA^{3-}$)			a	b	c	d	e	f	SSE	R2	Adj R2	RMSE
NPQ	acute	dark	0.114 (-0.214, 0.441)	-0.231 (-2.333, 1.872)	0.05728 (-0.1045, 0.219)	2.929 (0.352, 5.506)			0.426	0.828	0.794	0.168
		25 PAR	0.3655 (-0.4163, 1.147)	-0.251 (-1.794, 1.292)	0.162 (-0.254, 0.580)	2.774 (0.434, 5.115)			2.411	0.827	0.793	0.401
		65 PAR	0.490 (-0.381, 1.361)	-0.297 (-1.548, 0.954)	0.318 (-0.203, 0.840)	2.542 (1.056, 4.027)			3.115	0.901	0.881	0.456
	24h	dark	1100.000	-800.000	20.840	86.970	-0.193	-9.020	0.194	0.712	0.601	0.122
		25 PAR	1000.000	-793.000	20.920	86.840	-0.193	-8.283	0.483	0.820	0.750	0.193
		65 PAR	1000.000	-800.000	20.700	86.180	-0.153	-7.764	0.711	0.864	0.812	0.234
	48h	dark	549.254	-349.255	1059.019	4784.742	0.054	-8.809	0.041	0.637	0.485	0.058
		25 PAR	598.099	-398.091	41.702	176.943	0.018	-7.450	0.330	0.789	0.700	0.166
		65 PAR	661.189	-461.189	36.082	143.069	-0.046	-7.201	0.457	0.874	0.822	0.195
	week	dark	1.189	0.638	3.031	11.030	-0.109	-0.432	0.054	0.735	0.625	0.067
		25 PAR	1000.000	-793.000	24.110	85.430	-0.293	-8.191	0.095	0.965	0.951	0.089
		65 PAR	1000.000	-800.000	23.940	84.990	-0.315	-7.699	0.210	0.975	0.964	0.132
	rec	dark	640.087	-440.087	21.184	81.532	0.188	-8.215	0.010	0.974	0.964	0.028
		25 PAR	932.577	-732.577	24.007	85.001	-0.160	-8.038	0.008	0.995	0.993	0.026
		65 PAR	1013.078	-813.078	23.970	85.161	-0.170	-7.993	0.071	0.971	0.958	0.077

Ni^{2+}			a	b	c	d	e	f	SSE	R2	Adj R2	RMSE
NPQ	acute	dark	0.005 (-0.037, 0.047)	0.673 (-0.789, 2.134)	0.166 (0.020, 0.312)	-0.051 (-0.206, 0.104)			0.279	0.241	0.098	0.132
		25 PAR	0.755 (0.632, 0.878)	0.0226 (-0.0312, 0.0765)	0.002 (0.0016, 0.0050)	0.677 (-0.131, 1.486)			0.491	0.561	0.473	0.181
		65 PAR	0.828 (0.586, 1.071)	-0.029 (-0.130, 0.073)	0.006 (-0.035, 0.048)	0.845 (-0.185, 1.876)			0.366	0.711	0.653	0.156
	24h	dark	32303.647	-32103.148	34.698	201.710	-0.100	-12.246	0.298	0.406	0.158	0.158
		25 PAR	9601.208	-9401.224	2.248	12.464	-0.168	-10.274	1.170	0.616	0.456	0.312
		65 PAR	12770.694	-12570.705	2.444	13.401	-0.120	-10.116	1.494	0.601	0.435	0.353
	48h	dark	1000.000	-800.000	14.370	80.810	-0.105	-8.459	0.503	0.564	0.383	0.205
		25 PAR	7759.467	-7559.453	15.103	82.727	-0.113	-9.858	1.238	0.735	0.625	0.321
		65 PAR	23011.329	-22811.339	4.829	25.801	-0.154	-10.815	2.465	0.710	0.589	0.453
	week	dark	1914.822	-2614.855	43.588	207.446	-0.027	-9.453	0.353	0.628	0.472	0.171
		25 PAR	356.112	-1056.152	163.832	809.857	-0.008	-7.943	0.763	0.477	0.260	0.252
		65 PAR	592.084	-392.082	142.839	705.355	0.013	-7.328	0.357	0.817	0.741	0.172
	rec	dark	1.227	0.763	325.116	1619.808	0.330	1.437	0.117	0.797	0.712	0.099
		25 PAR	2149.990	-1950.001	34.376	162.806	-0.054	-8.818	0.212	0.893	0.848	0.133
		65 PAR	3723.977	-3523.981	38.679	180.888	-0.077	-9.239	0.396	0.871	0.817	0.182

891

$HAsO_4^{-2}/H_2AsO_4^-$			a	b	c	d	e	f	SSE	R2	Adj R2	RMSE
NPQ	acute	dark	n.d.	n.d.	n.d.	n.d.	n.d.	n.d.	n.d.	n.d.	n.d.	n.d.
		25 PAR	0.539 (-0.163, 1.245)	-0.058 (-0.382, 0.266)	0.048 (-0.265, 0.361)	0.699 (-0.577, 1.975)			0.646	0.668	0.597	0.215
		65 PAR	0.422 (-0.277, 1.121)	-0.172 (-0.576, 0.233)	0.142 (-0.163, 0.447)	0.617 (0.184, 1.049)			0.469	0.877	0.850	0.183
	24h	dark	0.862 (0.725, 0.999)	0.028 (-0.023, 0.080)	4.7e-08 (-2.5e-06, 2.6e-06)	3.551 (-9.113, 16.225)			0.053	0.370	0.236	0.062
		25 PAR	2.3e-11 (-5.3e-09, 5.4e-09)	5.083 (-47.044, 57.250)	0.602 (0.456, 0.748)	0.058 (-0.021, 0.136)			0.685	0.311	0.164	0.221
		65 PAR	4.9e-08 (-2.5e-06, 2.6e-06)	3.537 (-8.263, 15.345)	0.862 (0.736, 0.988)	0.029 (-0.019, 0.076)			0.508	0.413	0.288	0.191
	48h	dark	n.d.	n.d.	n.d.	n.d.			n.d.	n.d.	n.d.	n.d.
		25 PAR	0.648 (0.184, 1.112)	0.005 (-0.178, 0.187)	0.019 (-0.196, 0.234)	0.737 (-1.474, 2.949)			0.322	0.603	0.519	0.152
		65 PAR	0.888 (0.645, 1.131)	0.060 (-0.028, 0.149)	0.001 (-0.024, 0.026)	1.304 (-3.149, 5.757)			0.576	0.692	0.625	0.203
	week	dark	n.d.	n.d.	n.d.	n.d.	n.d.	n.d.	n.d.	n.d.	n.d.	n.d.
		25 PAR	n.d.	n.d.	n.d.	n.d.	n.d.	n.d.	n.d.	n.d.	n.d.	n.d.
		65 PAR	n.d.	n.d.	n.d.	n.d.	n.d.	n.d.	n.d.	n.d.	n.d.	n.d.
	rec	dark	n.d.	n.d.	n.d.	n.d.	n.d.	n.d.	n.d.	n.d.	n.d.	n.d.
		25 PAR	n.d.	n.d.	n.d.	n.d.	n.d.	n.d.	n.d.	n.d.	n.d.	n.d.
		65 PAR	n.d.	n.d.	n.d.	n.d.	n.d.	n.d.	n.d.	n.d.	n.d.	n.d.

892

Pb^{2+}			a	b	c	d	e	f	SSE	R2	Adj R2	RMSE
NPQ	acute	dark	n.d.	n.d.	n.d.	n.d.	n.d.	n.d.	n.d.	n.d.	n.d.	n.d.
		25 PAR	n.d.	n.d.	n.d.	n.d.	n.d.	n.d.	n.d.	n.d.	n.d.	n.d.
		65 PAR	n.d.	n.d.	n.d.	n.d.	n.d.	n.d.	n.d.	n.d.	n.d.	n.d.
	24h	dark	n.d.	n.d.	n.d.	n.d.	n.d.	n.d.	n.d.	n.d.	n.d.	n.d.
		25 PAR	n.d.	n.d.	n.d.	n.d.	n.d.	n.d.	n.d.	n.d.	n.d.	n.d.
		65 PAR	1.528 (-0.292, 3.348)	0.464 (-0.303, 1.234)	0.001 (0.0001, 0.003)	-1.325 (-1.919, -0.720)			0.062	0.720	0.657	0.083
	48h	dark	n.d.	n.d.	n.d.	n.d.	n.d.	n.d.	n.d.	n.d.	n.d.	n.d.
		25 PAR	n.d.	n.d.	n.d.	n.d.	n.d.	n.d.	n.d.	n.d.	n.d.	n.d.
		65 PAR	n.d.	n.d.	n.d.	n.d.	n.d.	n.d.	n.d.	n.d.	n.d.	n.d.
	week	dark	0.001 (-0.413, 0.414)	-1.701 (-150.955, 147.573)	1.784 (-42.013, 45.570)	1.037 (-21.42, 23.5)			0.095	0.607	0.459	0.109
		25 PAR	0.159 (-2.482, 2.804)	-0.320 (-4.461, 3.821)	20.5 (-489.2, 530.2)	2.724 (-19.222, 24.661)			0.080	0.404	0.180	0.100
		65 PAR	3.04e+04 (-1.4e+06 ,1.5e+06)	8.407 (-26.554, 43.363)	0.670 (0.027, 1.313)	0.022 (-0.240, 0.285)			0.078	0.542	0.371	0.099
	rec	dark	n.d.	n.d.	n.d.	n.d.	n.d.	n.d.	n.d.	n.d.	n.d.	n.d.
		25 PAR	n.d.	n.d.	n.d.	n.d.	n.d.	n.d.	n.d.	n.d.	n.d.	n.d.
		65 PAR	n.d.	n.d.	n.d.	n.d.	n.d.	n.d.	n.d.	n.d.	n.d.	n.d.

893

Table 3. Parameters and fit goodness coefficients of YII concentration-response curves for heavy metal exposed samples. Hormetic model (x) = ((a- b)./(1+(exp((c* x)-d)))./(1+(exp((e*x)- f))). DFE: 12 for As, Cu, Ni, Zn; DFE: 8 for Pb. Fit parameters in Matlab: MaxFunEvals = 6000; MaxIter = 40000; Robust = 'Bisquare'.

Zn^{2+}			a	b	c	d	e	f	SSE	R^2	Adj R^2	RMSE
YII	dark	acute	n.d.	n.d.	n.d.	n.d.	n.d.	n.d.	n.d.	n.d.	n.d.	n.d.
		24h	5.402	3.968	2.242	12.120	-0.003	-0.521	0.025	0.924	0.892	0.045
		48h	0.269	-0.630	2.637	14.360	0.029	0.416	0.007	0.974	0.963	0.024
		week	6.577	5.423	-0.004	-0.075	15.280	78.170	0.009	0.991	0.987	0.028
		rec	n.d.	n.d.	n.d.	n.d.	n.d.	n.d.	n.d.	n.d.	n.d.	n.d.
	25	acute	0.697	-0.197	0.015	0.017	1.039	7.966	0.002	0.873	0.820	0.012
		24h	0.712	-0.418	2.517	12.300	0.020	-0.434	0.013	0.964	0.949	0.033
		48h	0.345	-0.476	1.634	8.352	0.015	0.116	0.012	0.952	0.932	0.031
		week	0.239	-0.218	0.189	56.000	7.944	41.280	0.017	0.974	0.963	0.037
		rec	n.d.	n.d.	n.d.	n.d.	n.d.	n.d.	n.d.	n.d.	n.d.	n.d.
	65	acute	0.903	0.079	-0.138	0.578	0.196	0.865	0.006	0.739	0.631	0.022
		24h	1.139	0.129	-0.300	0.317	0.465	0.726	0.053	0.789	0.701	0.066
		48h	0.556	-0.247	-0.231	0.387	0.445	1.103	0.045	0.748	0.643	0.062
		week	220.000	90.000	26.460	133.900	0.018	-5.847	0.012	0.972	0.960	0.031
		rec	1.176	0.439	0.039	0.954	0.044	0.903	0.009	0.571	0.392	0.028

Cu (except $CuHPO_4$ aq, $CuEDTA^{3-}$)			a	b	c	d	e	f	SSE	R2	Adj R2	RMSE
YII	dark	acute	1.525	-0.428	0.112	0.128	-0.136	0.122	0.003	0.355	0.086	0.016
		24h	223.917	87.018	41.246	178.407	0.022	-5.561	0.008	0.992	0.988	0.027
		48h	369.974	-58.952	37.629	162.658	0.014	-6.658	0.006	0.995	0.993	0.021
		week	412.000	-100.000	3.579	13.870	-0.031	-6.828	0.134	0.886	0.838	0.106
		rec	440.800	440.200	4.549	17.000	0.343	10.670	0.085	0.942	0.918	0.084
	25	acute	-4.594	-5.115	-0.080	2.152	1.049	6.655	0.027	0.612	0.451	0.048
		24h	0.913	0.466	3.883	18.600	3.891	18.610	0.063	0.914	0.879	0.073
		48h	-2.461	-2.900	6.011	29.860	6.491	32.080	0.031	0.957	0.940	0.050
		week	0.522	-0.641	3.217	13.570	0.003	-0.401	0.092	0.884	0.835	0.088
		rec	3.379	2.425	5.455	22.820	0.028	0.090	0.051	0.950	0.929	0.065
	65	acute	1.221	-0.055	-0.022	-0.839	1.222	6.589	0.015	0.865	0.809	0.035
		24h	0.822	0.046	-0.010	-0.094	3.014	12.890	0.093	0.818	0.742	0.088
		48h	0.176	-0.560	0.016	-0.147	10.270	46.010	0.006	0.988	0.984	0.022
		week	199.900	-199.900	7.459	30.070	0.011	-6.972	0.007	0.988	0.983	0.024
		rec	0.892	0.496	7.611	31.530	7.032	29.340	0.011	0.983	0.976	0.030

Ni^{2+}			a	b	c	d	e	f	SSE	R^2	Adj R^2	RMSE
YII	dark	acute	n.d.	n.d.	n.d.	n.d.	n.d.	n.d.	n.d.	n.d.	n.d.	n.d.
		24h	0.429	-0.141	0.904	5.332	-0.013	2.618	0.024	0.854	0.793	0.045
		48h	195.000	115.000	24.010	131.000	0.054	-5.091	0.043	0.910	0.872	0.060
		week	0.692	-0.107	1.765	6.838	0.019	1.092	0.049	0.955	0.937	0.064
		rec	309.000	1.001	10.320	47.940	0.008	-6.211	0.014	0.990	0.986	0.034
	25	acute	n.d.	n.d.	n.d.	n.d.	n.d.	n.d.	n.d.	n.d.	n.d.	n.d.
		24h	1.016	-0.429	0.417	0.267	-0.323	0.280	0.028	0.905	0.866	0.049
		48h	0.532	0.068	361.000	2000.000	0.757	2.872	0.019	0.958	0.940	0.040
		week	0.815	0.061	-0.030	0.687	1.736	6.080	0.017	0.978	0.969	0.038
		rec	0.554	0.036	35.230	163.800	2.254	10.800	0.005	0.994	0.992	0.021
	65	acute	n.d.	n.d.	n.d.	n.d.	n.d.	n.d.	n.d.	n.d.	n.d.	n.d.
		24h	0.831	-0.051	0.476	0.731	-0.232	0.332	0.024	0.875	0.822	0.045
		48h	1.104	-0.044	0.602	0.508	-0.363	0.184	0.023	0.928	0.898	0.043
		week	0.668	-0.387	0.841	1.101	-0.436	0.375	0.020	0.960	0.944	0.040
		rec	1.126	0.349	1.154	4.311	-0.147	0.251	0.157	0.726	0.612	0.115

$HAsO_4^{-2}/H_2AsO_4^-$			a	b	c	d	e	f	SSE	R2	Adj R2	RMSE
YII	dark	acute	n.d.	n.d.	n.d.	n.d.	n.d.	n.d.	n.d.	n.d.	n.d.	n.d.
		24h	n.d.	n.d.	n.d.	n.d.	n.d.	n.d.	n.d.	n.d.	n.d.	n.d.
		48h	n.d.	n.d.	n.d.	n.d.	n.d.	n.d.	n.d.	n.d.	n.d.	n.d.
		week	n.d.	n.d.	n.d.	n.d.	n.d.	n.d.	n.d.	n.d.	n.d.	n.d.
		rec	n.d.	n.d.	n.d.	n.d.	n.d.	n.d.	n.d.	n.d.	n.d.	n.d.
	25	acute	2.364	-1.078	0.497	2.786	-0.026	-1.816	0.005	0.815	0.738	0.019
		24h	1.238	0.048	2.036	10.796	0.006	-0.545	0.018	0.274	-0.028	0.039
		48h	1.117	-0.296	0.235	0.232	-0.218	0.539	0.010	0.695	0.568	0.029
		week	1.389	-0.103	1.513	10.557	0.011	-0.758	0.011	-0.015	-0.438	0.030
		rec	n.d.	n.d.	n.d.	n.d.	n.d.	n.d.	n.d.	n.d.	n.d.	n.d.
	65	acute	1.860	-0.574	0.540	2.457	-0.047	-1.640	0.007	0.753	0.649	0.024
		24h	1.210	0.076	1.780	9.262	-0.002	-0.831	0.012	0.424	0.185	0.032
		48h	1.390	-0.104	0.636	3.395	-0.026	-1.049	0.009	0.656	0.513	0.028
		week	n.d.	n.d.	n.d.	n.d.	n.d.	n.d.	n.d.	n.d.	n.d.	n.d.
		rec	n.d.	n.d.	n.d.	n.d.	n.d.	n.d.	n.d.	n.d.	n.d.	n.d.

901

Pb^{2+}			a	b	c	d	e	f	SSE	R^2	Adj R^2	RMSE
YII	dark	acute	402.234	-91.234	6.000	33.000	0.029	-6.836	0.003	0.485	0.056	0.021
		24h	401.183	-90.184	6.000	33.000	0.040	-6.836	0.004	0.572	0.215	0.026
		48h	409.168	-98.168	6.000	33.000	0.023	-6.817	0.007	0.110	-0.632	0.033
		week	417.016	-106.016	6.000	33.000	0.021	-6.793	0.001	0.561	0.195	0.014
		rec	422.638	-111.638	6.000	33.000	0.004	-6.781	0.005	-0.143	-1.095	0.029
	25	acute	1.490	0.206	0.700	33.000	0.036	-0.653	0.004	0.153	-0.553	0.025
		24h	1.028	-0.554	0.056	-0.039	0.044	0.260	0.005	0.523	0.125	0.028
		48h	1.176	-0.326	6.000	33.000	0.056	-0.859	0.006	0.246	-0.383	0.032
		week	1.044	0.456	6.000	33.000	0.202	1.286	0.005	0.217	-0.436	0.028
		rec	0.607	-0.092	6.000	33.000	-0.017	0.876	0.010	-1.479	-3.544	0.041
	65	acute	0.936	0.262	3.475	3.715	0.031	0.142	0.003	0.123	-0.609	0.022
		24h	0.993	-0.670	4.369	2.983	0.053	-1.265	0.018	-0.513	-1.774	0.055
		48h	0.907	-0.180	10.630	-11.940	0.052	-0.688	0.004	0.325	-0.237	0.025
		week	0.443	0.051	5.984	0.449	2.119	-0.546	0.003	0.209	-0.450	0.021
		rec	355.077	-44.077	6.000	33.000	-0.059	-6.981	0.021	0.016	-0.805	0.060

902

Table 4. Parameters and fit goodness coefficients of F_0 concentration-response curves for heavy metal exposed samples. Hormetic model (x) = ((a- b)./(1+(exp((c* x)-d)))./(1+(exp((e*x)- f))). DFE: 12 for As, Cu, Ni, Zn; DFE: 6 for Pb. Linear model: f(x) = a+b*x, DFE: 16. Coefficients 95% confidence bounds in parenthesis (only for linear fit). Fit parameters in Matlab: MaxFunEvals = 6000; MaxIter = 40000; Robust = 'Bisquare'.

Zn^{2+}			a	b	c	d	e	f	SSE	R^2	Adj R^2	RMSE
F_0	dark	acute	n.d.	n.d.	n.d.	n.d.	n.d.	n.d.	n.d.	n.d.	n.d.	n.d.
		24h	10720.000	632.700	3.847	20.340	-0.048	-3.487	48059.223	0.766	0.669	63.285
		48h	-60.820	-407.200	1.887	54.940	2.950	14.970	43770.475	0.830	0.759	60.395
		week	-5408.000	-5774.000	0.371	1.777	41.940	211.600	18047.582	0.940	0.915	38.781
		rec	9000.000	-9000.000	13.720	73.750	-0.016	-3.894	27351.509	0.896	0.853	47.742
	25	acute	n.d.	n.d.	n.d.	n.d.	n.d.	n.d.	n.d.	n.d.	n.d.	n.d.
		24h	121.300	-119.600	3.211	17.130	-20.280	76.170	24457.626	0.760	0.661	45.146
		48h	136.200	-135.100	3.767	105.900	2.134	10.460	16795.467	0.886	0.839	37.412
		week	-398.500	-713.400	41.240	207.600	0.299	1.337	6835.469	0.965	0.951	23.867
		rec	2807.000	807.100	6.670	35.780	-0.012	-1.710	20006.710	0.885	0.836	40.832
	65	acute	n.d.	n.d.	n.d.	n.d.	n.d.	n.d.	n.d.	n.d.	n.d.	n.d.
		24h	947.800	735.600	3.101	16.760	21.870	128.000	12867.157	0.813	0.735	32.745
		48h	1067.000	458.800	0.020	-0.414	2.251	11.260	11890.636	0.897	0.855	31.478
		week	-224.500	-516.600	0.320	1.432	122.300	614.400	6680.165	0.962	0.946	23.594
		rec	143.400	-143.100	0.154	33.000	6.534	35.150	23656.322	0.843	0.777	44.400

Cu (except $CuHPO_4$ aq, $CuEDTA^{3-}$)			a	b	c	d	e	f	SSE	R2	Adj R2	RMSE
F0	dark	acute	n.d.	n.d.	n.d.	n.d.	n.d.	n.d.	n.d.	n.d.	n.d.	n.d.
		24h	141.221	-171.243	3.041	10.747	150.196	675.129	22142.273	0.937	0.911	42.956
		48h	164.248	-194.299	2.740	9.379	120.886	541.528	23821.752	0.948	0.927	44.555
		week	162.678	-192.679	3.719	12.170	692.427	3141.112	9687.127	0.979	0.970	28.412
		rec	180.917	-210.917	3.922	12.516	43.887	179.303	16409.369	0.972	0.960	36.979
	25	acute	280.028	30.958	0.973	58.671	1.066	5.481	37492.739	0.478	0.261	55.896
		24h	597.800	-597.800	-0.069	-1.150	4.128	15.760	11616.011	0.954	0.934	31.113
		48h	989.400	-489.400	-0.055	-1.328	3.272	12.390	7838.525	0.973	0.962	25.558
		week	968.500	463.700	-0.068	0.478	10.590	40.570	3169.474	0.990	0.986	16.252
		rec	369.700	-130.100	13.080	49.970	-0.223	1.105	2677.920	0.994	0.991	14.939
	65	acute	269.365	40.654	2.076	53.040	1.136	5.446	43727.636	0.364	0.099	60.365
		24h	270.774	39.206	2.076	53.040	4.412	15.370	17125.141	0.914	0.878	37.777
		48h	286.002	23.939	2.076	53.040	3.533	12.096	15561.382	0.938	0.912	36.011
		week	290.010	20.010	2.076	53.040	21.650	73.911	2510.316	0.991	0.987	14.464
		rec	315.510	-5.490	2.076	53.040	21.071	71.749	10229.705	0.975	0.964	29.197

Ni^{2+}			a	b	c	d	e	f	SSE	R^2	Adj R^2	RMSE
F_0	dark	acute	n.d.	n.d.	n.d.	n.d.	n.d.	n.d.	n.d.	n.d.	n.d.	n.d.
		24h	-1139.000	-1518.000	0.140	10.500	1.699	8.434	14091.176	0.937	0.911	34.268
		48h	188.500	-188.200	-8.919	96.260	1.523	6.826	93362.763	0.764	0.666	88.206
		week	366.000	-155.800	43.430	209.900	0.576	1.073	67334.897	0.913	0.877	74.908
		rec	1220.000	419.700	4.459	19.430	0.130	-0.002	41613.506	0.942	0.918	58.888
	25	acute	n.d.	n.d.	n.d.	n.d.	n.d.	n.d.	n.d.	n.d.	n.d.	n.d.
		24h	5146.000	-4794.000	1.491	7.456	0.051	-3.533	16641.842	0.913	0.877	37.240
		48h	-431.600	-1183.000	2.753	14.020	0.163	-0.794	30443.718	0.876	0.824	50.368
		week	918.471	-607.471	1.858	7.207	0.118	-1.349	31937.082	0.940	0.915	51.589
		rec	-328.600	-1082.000	4.189	17.920	0.108	-0.216	27964.813	0.945	0.922	48.274
	65	acute	n.d.	n.d.	n.d.	n.d.	n.d.	n.d.	n.d.	n.d.	n.d.	n.d.
		24h	6774.000	-6757.000	1.461	7.419	0.052	-3.977	9789.021	0.931	0.902	28.561
		48h	443.700	-175.400	2.642	13.600	0.199	-0.566	31716.951	0.871	0.817	51.411
		week	-141.300	-545.300	0.644	1.145	33.700	164.200	26444.064	0.944	0.921	46.943
		rec	1105.000	610.100	0.231	0.651	5.920	25.730	25581.848	0.949	0.927	46.172

910

$HAsO_4^{-2}/H_2AsO_4^-$			a	b	c	d	e	f	SSE	R2	Adj R2	RMSE
F0	dark	acute	n.d.	n.d.					n.d.	n.d.	n.d.	n.d.
		24h	n.d.	n.d.					n.d.	n.d.	n.d.	n.d.
		48h	n.d.	n.d.					n.d.	n.d.	n.d.	n.d.
		week	n.d.	n.d.					n.d.	n.d.	n.d.	n.d.
		rec	n.d.	n.d.					n.d.	n.d.	n.d.	n.d.
	25	acute	279.650 (250.843, 308.360)	-9.847 (-1801, -1.691)					20829.965	0.430	0.395	36.081
		24h	275.204 (248.604, 301.762)	-13.640 (-21.160, -6.114)					35383.052	0.428	0.392	47.026
		48h	247.601 (225.943, 269.312)	-5.648 (-11.801, 0.501)					23643.819	0.617	0.593	38.441
		week	344.756 (315.512, 373.834)	-15.071 (-23.332, -6.815)					42616.018	0.443	0.408	51.609
		rec	378.641 (345.805, 411.362)	-5.474 (-14.763, 3.814)					53898.149	-0.019	-0.083	58.040
	65	acute	254.632 (234.208, 274.900)	-10.361 (-16.133, -4.588)					20829.965	0.430	0.395	36.081
		24h	249.634 (227.407, 271.809)	-11.54 (-17.83, -5.251)					24746.682	0.425	0.389	39.328
		48h	230.317 (210.103, 250.532)	-6.709 (-12.43, -0.985)					20495.026	0.714	0.697	35.790
		week	319.644 (298.607, 340.632)	-15.541 (-21.494, -9.583)					22178.829	0.650	0.628	37.231
		rec	366.101 (337.126, 395.143)	-6.068 (-14.294, 2.153)					42265.079	0.016	-0.045	51.396

911

Pb^{2+}			a	b	c	d	e	f	SSE	R^2	Adj R^2	RMSE
F_0	dark	acute	2253.182	-1936.182	55.288	-74.759	0.070	-2.466	35722.219	0.178	-0.507	77.160
		24h	825.633	-508.633	57.295	-77.865	0.071	-1.222	8946.170	0.504	0.090	38.614
		48h	184.100	-182.100	29.290	-32.160	36.830	-49.130	64990.804	0.049	-0.743	104.076
		week	1532.000	-1215.000	73.760	-80.180	0.156	-2.086	21664.486	0.600	0.266	60.089
		rec	9082.172	-8765.172	261.409	270.913	0.138	-3.700	209574.537	0.147	-0.564	186.893
	25	acute	1325.420	-1325.420	0.046	-2.109	60.312	-82.047	24292.279	0.041	-0.758	63.629
		24h	172.000	-170.800	0.535	0.535	25.360	-33.530	5208.224	0.692	0.435	29.462
		48h	1255.861	-1255.861	0.041	-2.066	63.364	-85.883	37325.499	0.070	-0.705	78.873
		week	4581.599	-4581.599	0.166	-3.678	4103.939	4857.713	39939.508	0.385	-0.128	81.588
		rec	3195.394	-3195.394	0.100	-2.840	1508531.750	2067289.404	87958.108	0.043	-0.755	121.077
	65	acute	195.100	-193.100	18.750	-22.010	0.368	0.164	13598.167	0.342	-0.206	47.606
		24h	169.200	-167.200	11.290	-13.680	0.856	-0.245	5219.820	0.722	0.490	29.495
		48h	1667.868	-1665.868	62.764	-84.996	0.054	-2.487	33630.375	0.111	-0.630	74.867
		week	2829.000	-2828.000	11.760	7.394	0.188	-3.262	34458.581	0.478	0.043	75.783
		rec	1453.000	-1453.000	0.103	-2.103	8.040	11.650	79829.032	-0.369	-1.509	115.347

912